

A RATIONAL APPROACH TO THE USE OF PRANDTL'S MIXING
LENGTH MODEL IN FREE TURBULENT
SHEAR FLOW CALCULATIONS

By David H. Rudy and Dennis M. Bushnell
NASA Langley Research Center

SUMMARY

Prandtl's basic mixing length model was used to compute 22 of the 24 test cases for the Langley Working Conference on Free Turbulent Shear Flows. The calculations employed appropriate algebraic length scale equations and single values of mixing length constant for planar and axisymmetric flows, respectively. Good agreement with data was obtained except for flows, such as supersonic free shear layers, where large sustained density changes occur. The inability to predict the more gradual mixing in these flows is tentatively ascribed to the presence of a significant turbulence-induced transverse static-pressure gradient which is neglected in conventional solution procedures. Some type of an equation for length scale development was found to be necessary for successful computation of highly nonsimilar flow regions such as jet or wake development from thick wall flows.

SYMBOLS

c_p	specific heat at constant pressure
$\overline{c_p} = \frac{c_p}{c_{p,e}}$	
D	nozzle diameter
j	geometry parameter, 0 or 1 for two-dimensional or axisymmetric flow, respectively
k	thermal conductivity
l	mixing length
l_{sd}	mixing length associated with second-derivative term in equation (5)

l/δ	mixing length constant
M	Mach number
N_{Pr}	Prandtl number, $\mu c_p/k$
N_{Sc}	Schmidt number
p	static pressure
Δp	static-pressure difference across shear layer
R	constant in equation of state for a perfect gas
R_b	Reynolds number based on characteristic body dimension, $\mu_e u_e r_b / \rho_e$
r	radial coordinate
$\bar{r} = \frac{r}{r_b}$	
r_b	characteristic body dimension
T	static temperature
$\bar{T} = \frac{T}{T_e}$	
u	mean velocity in streamwise direction
$\bar{u} = \frac{u}{u_e}$	
$\overline{u'v'}$	turbulent shear stress
v	mean velocity in transverse direction
$\overline{v'}$	fluctuating velocity in transverse direction
$w = 1 - \frac{u}{u_e}$	

x streamwise coordinate in physical plane

$$\bar{x} = \frac{x}{r_b}$$

y transverse coordinate in physical plane

$$\bar{y} = \frac{y}{r_b}$$

$\left. \begin{array}{l} \bar{y}.01, \bar{y}.05, \bar{y}.95 \\ \bar{y}.99, \bar{y}.995 \end{array} \right\}$ value of \bar{y} where $\frac{u - u_{\zeta}}{u_e - u_{\zeta}} = 0.01, 0.05, 0.95, 0.99, 0.995$, respectively

α concentration

β mixing angle in wake flows

γ ratio of specific heats

δ width of mixing region

$$\bar{\delta} = \frac{\delta}{r_b}$$

ϵ eddy kinematic viscosity

ζ streamwise Von Mises coordinate

$$\bar{\zeta} = \frac{\zeta}{r_b}$$

θ momentum thickness

μ dynamic viscosity

$$\bar{\mu} = \frac{\mu}{\mu_e}$$

ρ density

$$\bar{\rho} = \frac{\rho}{\rho_e}$$

σ spreading parameter

σ_0	spreading parameter when $\frac{u_2}{u_1} = 0$ and $M \rightarrow 0$
τ	transverse Von Mises coordinate; or shear stress
$\bar{\tau}$	nondimensional transverse Von Mises coordinate, $\frac{\tau}{(\rho_e u_e)^{1/1+j} r_b}$
ϕ	mixing angle for jet flows

Subscripts:

c	end of potential core
t	center line
e	external stream
i	initial
ip	inflection point
j	jet exit plane
l	laminar
n	nth species
p	primary flow
s	secondary flow
t	turbulent
1	high-velocity side of shear layer
2	low-velocity side of shear layer
I,II	regions I and II in jet flows (figs. 2 and 4) and wake flows (fig. 3)
III	region III in jet flows (figs. 2 and 4)

Superscript:

j geometry parameter where $j = 0$ in two-dimensional flows and $j = 1$ in axisymmetric flows

THE MIXING LENGTH CONCEPT

The classic phenomenological model for the turbulent shear stress is the mixing length theory (refs. 1 and 2) developed by L. Prandtl in 1925. Although the model lacks a rigorous physical basis, it has nonetheless proved to be quite successful in both boundary-layer and free shear flow calculations.

In formulating his model, Prandtl assumed that the Reynolds stress is produced by momentum transfer normal to the mean flow direction from regions of high momentum to regions of low momentum. The mixing length l is then defined (in rough analogy to the mean free path of a molecule) to be the average distance over which a fluid element transfers momentum. A detailed description of the model's theoretical development is available in many texts (e.g., ref. 3, p. 277 and ref. 4, p. 545).

Mathematically, for quasi-parallel shear flows the eddy viscosity is expressed as the product of the square of the mixing length and the absolute value of the local mean velocity gradient, that is,

$$\epsilon = l^2 \left| \frac{\partial u}{\partial y} \right| \quad (1)$$

Therefore, the turbulent shear stress for two-dimensional or axisymmetric flow becomes

$$\tau_t = -\overline{\rho u'v'} = \rho \epsilon \frac{\partial u}{\partial y} = \rho l^2 \left| \frac{\partial u}{\partial y} \right| \frac{\partial u}{\partial y} \quad (2)$$

where the mixing length is generally taken to be the product of an empirically determined constant and some characteristic scale of the mixing region, that is,

$$l = \text{Constant} \times \delta$$

or

$$\text{Constant} = \frac{l}{\delta} \quad (3)$$

Thus,

$$\tau_t = \rho \left(\frac{l}{\delta} \right)^2 \delta^2 \left| \frac{\partial u}{\partial y} \right| \left| \frac{\partial u}{\partial y} \right| \quad (4)$$

Equation (4) has been widely used in the calculation of a variety of flows with both analytical and numerical solution methods. After early use in pipe flow and flat-plate boundary-layer analytical solutions, the mixing length model has been particularly successful in the numerical computations of both incompressible (e.g., refs. 5 and 6) and compressible (e.g., refs. 7 and 8) turbulent boundary-layer flows with appropriate definitions of the mixing length specified for the "wall" and "wake" regions. For example, Patankar and Spalding (ref. 7) defined the mixing length as a numerical function of the distance from the wall and the boundary-layer thickness. Bushnell and Beckwith (ref. 9) then extended the use of the mixing length model to include the compressible nonequilibrium case.

A number of well-known approximate analytic solutions were developed for low-speed free flows by using Prandtl's mixing length model. Prandtl studied the smoothing of a velocity discontinuity (ref. 4, p. 687) and assumed similar velocity profiles. Tollmien assumed similarity and presented solutions for both the circular jet (ref. 4, p. 699) and the two-dimensional jet (ref. 4, p. 696) issuing into still surroundings as well as the two-dimensional two-stream mixing layer (ref. 4, p. 689). Schlichting (ref. 4, p. 691) in his thesis first examined the two-dimensional wake. Using measurements in the wake of a circular cylinder, he found l/δ to be 0.18. Kuethe (ref. 10) extended Tollmien's solution for the mixing region of a plane jet to the general case of the mixing of two parallel streams with different velocities. Kuethe also solved the problem of the mixing region surrounding an axisymmetric jet issuing into still surroundings by assuming local similarity. Using experimental measurements and taking the mixing length to be proportional to the width of the mixing region, he obtained $l/\delta = 0.0705$. Squire and Truncer (ref. 11) considered axisymmetric coaxial jets and used $l/\delta = 0.082$.

Several objections to the mixing length concept have been raised. For instance, according to equation (2) the eddy kinematic viscosity ϵ always vanishes at points of zero velocity gradient, a condition which is physically unrealistic (e.g., the center line of a jet or wake). Prandtl (ref. 1) recognized this difficulty and proposed that ϵ be considered proportional to a statistical mean of $\partial u/\partial y$ in the vicinity of a velocity maximum. The mixing length model for shear stress thus becomes

$$\tau_t = \rho l^2 \frac{\partial u}{\partial y} \left[\left(\frac{\partial u}{\partial y} \right)^2 + l_{sd}^2 \left(\frac{\partial^2 u}{\partial y^2} \right)^2 \right]^{1/2} \quad (5)$$

where l_{sd} is an additional length which must be determined experimentally. Equation (5) has seldom been used in analytical solutions because of the mathematical difficulties of including its more complex form. (There is no such problem if numerical solutions are employed.)

Another deficiency of the model given by equation (4) becomes evident in the study of the two-stream mixing layers. In this case the analytic solution exhibits a discontinuity in $\partial^2 u / \partial y^2$ at the mixing region boundaries instead of predicting the expected asymptotic approach of the mixing region velocity to the two free-stream values. Equation (5) is free of this problem.

In addition, the original assumption of constant mixing length across the mixing region has led to inaccurate predictions of the fluctuating components, according to Liepmann and Laufer (ref. 12), despite generally good agreement of the mean velocity profiles with experimental data.

Later Alexander, Baron, and Comings (ref. 13) demonstrated that Prandtl's original development required the assumption that the turbulence intensity and mixing length be isotropic. They concluded, however, that this first-order assumption did not seriously limit the application of the model. The original physical concept of a mixing length seemingly requires that its magnitude be small in comparison with mean flow dimensions. However, the fact that it has been found experimentally (ref. 14) that the mixing length is not small in comparison with mean flow dimensions is often considered a basic defect of the mixing length theory.

Recently several authors (e.g., ref. 15) have shown, by means of the turbulent kinetic energy approach, that the mixing length hypothesis implies that production equals dissipation of turbulence energy. Comparison of figures 6-9 and 7-44 in Hinze (ref. 3) shows that this assumption is much more defensible in boundary layers than in free shear flows.

Most investigators abandoned the mixing length in favor of Prandtl's later constant exchange coefficient eddy viscosity model (ref. 16), whose mathematical definition was more easily incorporated into analytical solutions. This "new" model overcame some of the difficulties of the mixing length model and gave slightly better agreement with experimental data. It has become historically the most widely used incompressible model.

Recently Elassar and Pandolfini (ref. 17) numerically investigated the compressible free shear layer in a backstep region and concluded that l/δ must have different values in the similar and nonsimilar regions. Wagner (ref. 18) used the mixing length model with the second-derivative term (eq. (5)) and $\frac{l}{\delta} = \frac{l_{sd}}{\delta} = 0.08$ to correctly predict the development of the hypersonic turbulent wake produced by a wedge.

The first attempt to systematically apply the mixing length model to a significant range of free turbulent flows was Harsha's study (ref. 19) of eddy viscosity models.

Harsha applied a single mixing length constant, 0.082 (the value used by Squire and Truncer (ref. 11)), to both compressible and incompressible flows. Apparently, for all regions except the potential core of a jet, he defined the width parameter to be twice the half-velocity radius (the radius for which $u = (u_t + u_e)/2$). In the shear-layer region of jets he used the width of the mixing region. This approach led to poor overall agreement with the selected experimental data although he obtained good prediction of the velocity potential core length for the subsonic circular jet and the subsonic coaxial air-air mixing cases. His predicted potential core was too short for the compressible jet issuing into still air and too long for hydrogen-air coaxial mixing flows with mass flow ratio $\rho_e u_e / \rho_j u_j$ greater than 2.0. For all these calculations, the asymptotic slope and the center-line velocity decay curve was underpredicted. However, the mixing length model did predict the early center-line velocity increase for both an axisymmetric and a two-dimensional subsonic wake very satisfactorily, although the downstream values were underpredicted in both cases.

THE "RATIONAL" APPROACH

The present effort was the result of a desire on the part of the conference organizers to have the mixing length eddy viscosity model compared with newer formulations. Recent success (refs. 9, 20, and 21) at Langley in the use of Prandtl's model in high-speed boundary layers indicated that the model should be given further consideration in free shear flows as well. Rather than repeat the Harsha approach (ref. 19) with the 24 conference test cases, an approach which might be termed a more "rational" approach was selected in which each class of flows would be given individual consideration. The designation "rational" merely indicates that the approach was designed to better represent the actual physics of free mixing than can be accomplished by conventional use of the basic model.

On the basis of boundary-layer experience, the so-called "rational" approach was, at the beginning of the investigation, visualized as the inclusion of the following modifications in the basic mixing length model (eq. (2)):

(1) A consistent set of values for the proportionality constant l/δ were to be used. Originally it seemed that this might involve a different constant for each region of a jet or wake. However, the results to be presented in this paper indicate a single value of l/δ for all two-dimensional flows and a single value for all axisymmetric flows, a conclusion in agreement with the experience of Spalding's group at Imperial College (refs. 15 and 22 and paper 11 of this compilation).

(2) Most importantly, a simple length scale equation would be included to provide a reasonable transition from the relatively small scale of turbulent motion in the shear layer of a jet to the larger scales of turbulence in the far field. Similar consideration would be given to wake and coaxial flows developing from wall flows. This approach had been successfully used in the slot injection studies of references 20 and 21.

(3) Recent experience (ref. 23) in turbulent-boundary-layer calculations has shown a pronounced increase in turbulent shear stress near the end of transition and the beginning of turbulent flow. This "low Reynolds number effect" was to be investigated for any relevant free shear flow test cases. However, for the test cases considered herein this effect was not included due to the lack of information concerning possible magnitudes and variations of the "low Reynolds number effect" in free turbulent flows.

(4) The use of an intermittency factor in the calculation procedure was to be explored. Wagner (ref. 18) had previously used intermittency in his hypersonic wake calculations.

(5) The effect of including the second-derivative term in the mixing length model (i.e., eq. (5)) would be studied for some of the test cases.

SOLUTION PROCEDURE AND TURBULENCE MODELS

Basic Equations

Solutions were obtained by using a computer code developed by Sinha, Fox, and Weinberger (refs. 24 and 25) for chemically nonreacting, quasi-parallel shear flows.

The boundary-layer equations with suitable boundary conditions are assumed to describe the motion of free shear flows. Only quasi-parallel flows are considered. Effects of longitudinal curvature and transverse pressure gradient are not included. For the mixing of dissimilar ideal gases the governing equations are as follows:

Conservation of mass

$$\frac{\partial}{\partial x}(\rho u y^j) + \frac{\partial}{\partial y}(\rho v y^j) = 0 \quad (6a)$$

Conservation of streamwise momentum

$$\rho u \frac{\partial u}{\partial x} + \rho v \frac{\partial u}{\partial y} = -\frac{\partial p_e}{\partial x} + \frac{1}{y^j} \frac{\partial}{\partial y} \left(\mu y^j \frac{\partial u}{\partial y} \right) \quad (6b)$$

Conservation of energy

$$\rho u c_p \frac{\partial T}{\partial x} + \rho v c_p \frac{\partial T}{\partial y} = u \frac{\partial p_e}{\partial x} + \frac{1}{y^j} \frac{\partial}{\partial y} \left(k y^j \frac{\partial T}{\partial y} \right) + \mu \left(\frac{\partial u}{\partial y} \right)^2 + \frac{\mu}{N_{Sc}} \sum_n \left(c_{p,n} \frac{\partial \alpha_n}{\partial y} \frac{\partial T}{\partial y} \right) \quad (6c)$$

Conservation of nth species

$$\rho u \frac{\partial \alpha_n}{\partial x} + \rho v \frac{\partial \alpha_n}{\partial y} = \frac{1}{y^j} \frac{\partial}{\partial y} \left(\frac{\mu}{N_{Sc}} y^j \frac{\partial \alpha_n}{\partial y} \right) \quad (6d)$$

where $j = 0$ or 1 for two-dimensional or axisymmetric flow, respectively. The associated boundary conditions are as follows:

At the center line ($y = 0$),

$$\frac{\partial u}{\partial y} = \frac{\partial T}{\partial y} = \frac{\partial \alpha_n}{\partial y} = 0 \quad (6e)$$

for all values of x .

At the edge of the mixing region,

$$\left. \begin{aligned} \lim_{y \rightarrow \infty} u(x,y) &= u_e \\ \lim_{y \rightarrow \infty} T(x,y) &= T_e \\ \lim_{y \rightarrow \infty} \alpha_n(x,y) &= \alpha_{n,e} \end{aligned} \right\} \quad (6f)$$

Equations (6a) to (6f) are solved in the modified Von Mises plane defined by the following transformation:

$$(1 + j) \tau^j \frac{\partial \tau}{\partial y} = \rho u y^j \quad (7a)$$

$$(1 + j) \tau^j \frac{\partial \tau}{\partial x} = -\rho v y^j \quad (7b)$$

and

$$\zeta = (1 + j)^{-2} \int_{x_i}^x \frac{dx}{R_b} \quad (8)$$

In the transformed plane only the momentum, energy, and species equations are needed since the continuity equation is inherently satisfied in the definition of the transformation. The transformed equations are then nondimensionalized with respect to external stream conditions and r_b , a characteristic length. It should be noted that Wagner (ref. 18) has shown the analysis of references 24 and 25 to be incorrect for longitudinal pressure gradient flows since the continuity equation was not satisfied by the non-dimensional Von Mises transformation used in that analysis. The correctly transformed equations of motion are as follows:

Momentum

$$\frac{\partial \bar{u}}{\partial \bar{\zeta}} = \frac{\bar{\tau}}{1 + j} \left(1 + M_e^2 \right) \frac{d(\ln u_e)}{d\bar{\zeta}} \frac{\partial \bar{u}}{\partial \bar{\tau}} + \left(\frac{1}{\bar{\rho} \bar{u}} - \bar{u} \right) \frac{d(\ln u_e)}{d\bar{\zeta}} + \frac{1}{\bar{\tau}^j} \frac{\partial}{\partial \bar{\tau}} \left(\bar{\rho} \bar{\mu} \bar{u} \frac{\bar{y}^{2j}}{\bar{\tau}^j} \frac{\partial \bar{u}}{\partial \bar{\tau}} \right) \quad (9a)$$

Energy

$$\begin{aligned} \frac{\partial \bar{T}}{\partial \bar{\zeta}} = & \frac{\bar{\tau}}{1 + j} \left(1 - M_e^2 \right) \frac{d(\ln u_e)}{d\bar{\zeta}} \frac{\partial \bar{T}}{\partial \bar{\tau}} + \frac{\bar{\tau}^{-j}}{c_p} \frac{\partial}{\partial \bar{\tau}} \left(\frac{\bar{\rho} \bar{\mu}}{N_{Pr}} \bar{u} \frac{\bar{y}^{2j}}{\bar{\tau}^j} \frac{\partial \bar{T}}{\partial \bar{\tau}} \right) + (\gamma_e - 1) M_e^2 \frac{d(\ln u_e)}{d\bar{\zeta}} \left(\bar{T} - \frac{1}{\bar{\rho} c_p} \right) \\ & + \frac{\bar{\rho} \bar{\mu} \bar{u}}{c_p} \left(\frac{\bar{y}}{\bar{\tau}} \right)^{2j} \left(\frac{\partial \bar{u}}{\partial \bar{\tau}} \right)^2 + \left(\frac{\bar{\rho} \bar{\mu}}{N_{Sc} c_p} \right) \left(\frac{\bar{y}}{\bar{\tau}} \right)^{2j} \bar{u} \frac{\partial \bar{T}}{\partial \bar{\tau}} \sum_n \frac{\partial \alpha_n}{\partial \bar{\tau}} \end{aligned} \quad (9b)$$

Species

$$\frac{\partial \alpha_n}{\partial \bar{\zeta}} = \frac{\bar{\tau}}{1 + j} \left(1 - M_e^2 \right) \frac{d(\ln u_e)}{d\bar{\zeta}} \frac{\partial \alpha_n}{\partial \bar{\tau}} + \bar{\tau}^{-j} \frac{\partial}{\partial \bar{\tau}} \left(\frac{\bar{\rho} \bar{\mu} \bar{u}}{N_{Sc}} \frac{\bar{y}^{2j}}{\bar{\tau}^j} \frac{\partial \alpha_n}{\partial \bar{\tau}} \right) \quad (9c)$$

Equations (9a) to (9c) were applied to turbulent flow by assuming that

$$\bar{\mu} = \bar{\mu}_l + \bar{\mu}_t \quad (10)$$

and by using turbulent Schmidt and Prandtl numbers. Suitable expressions were used for the laminar viscosity of the various gases used.

The flow was computed by using an implicit finite-difference technique (which is described in detail in refs. 24 and 25) to march downstream from the initial input profile.

Use of Von Mises Transformation

Apparently, most of the available computer codes for quasi-parallel free viscous flow solutions (e.g., refs. 7, 24, and 26) solve the boundary-layer equations in a Von Mises plane rather than the physical plane. For programing simplicity, a constant step size in the direction normal to the flow is usually assumed as in the procedure of reference 24. From equation (7a) this radial coordinate $\bar{\tau}$ in the method of reference 24 is defined by

$$\bar{\tau} = \left(\int_0^{\bar{y}} \bar{\rho} \bar{u} \bar{y}^j d\bar{y} \right)^{1/1+j} \quad (11)$$

Equation (11) shows that specifying equal $\Delta\bar{\tau}$ steps implies specifying equal increments of axial-direction mass flow across the computed region. Thus, larger steps (in terms of the physical plane) are located in regions of relatively low velocity (with respect to the free-stream or jet center-line velocity); this significantly reduces the accuracy in the crucial mixing regions. This problem is particularly evident in the calculation of compressible flows, especially the shear-layer calculations. As an example, in a typical Mach 5 two-dimensional shear-layer calculation with $u_2/u_1 = 0.05$, 49 of the 90 points across the mixing region profile are located in the region where u is approximately constant ($u/u_1 \cong 0.90$).

Turbulence Models

In accordance with the "rational approach" previously outlined, a conceptually simple (i.e., first order) model for the length scale variation in the streamwise direction was formulated for each of the major classes of flows. Thermal transport and mass transport were related to the momentum transport through the use of constant values of the turbulent Prandtl number and Schmidt number, respectively.

Two-dimensional shear layers. - Figure 1 shows the initial velocity profile used to generate the two-dimensional shear layers of test cases 1, 2, and 3. The same type of step profile was used for both the initial temperature and initial concentration profiles. Because of the inaccuracies introduced by the Von Mises transformation at the edge of the mixing region, the following definition for the width $\bar{\delta}$ of the region was necessary:

$$\bar{\delta} = (\text{Scaling factor}) (\bar{y}_{.95} - \bar{y}_{.05}) \quad (12)$$

where $\bar{y}_{.95}$ indicates the point in the mixing layer where $(u - u_{\zeta}) / (u_e - u_{\zeta}) = 0.95$. The scaling factor is necessary to obtain the "true" value of δ (i.e., $\bar{y}_{.99} - \bar{y}_{.01}$) and was taken to be 1.425 from the mean fit curve to the experimental data for two-stream mixing given by Halleen (ref. 27). This definition of width was used also for test case 5 and in the potential core region of all jet flows.

Since the initial boundary-layer profiles were given for test case 4, the two-dimensional version of the "coaxial jet length scale model" was applied to that case.

Jets into still air. - Figure 2 shows the length scale model developed for jets issuing into still air. The nondimensional mixing region width $\bar{\delta}$ is partially defined by the mixing angle ϕ . This definition allows a smooth transition between the relatively small mixing scale at the end of the potential core (which is designated region I) and the large scale turbulence downstream (region III).

For region I, $\bar{\delta}_I$ is given by equation (12); for region II,

$$\bar{\delta}_{II} = (\text{Scaling factor})(\bar{y}_{.95} - \bar{y}_{\zeta}) + (\bar{x} - \bar{x}_c) \tan \phi \quad (13)$$

where \bar{x}_c is the location of the end of the potential core. Region II extends to the point downstream at which $\bar{\delta}_{II}$ becomes $2(\text{Scaling factor})(\bar{y}_{.95} - \bar{y}_{\zeta})$. Finally, in region III,

$$\bar{\delta}_{III} = 2(\text{Scaling factor})(\bar{y}_{.95} - \bar{y}_{\zeta}) \quad (14)$$

The scaling factor for regions II and III was taken to be 1.2 from the similarity profile for a self-preserving jet given by Wygnanski and Fiedler (ref. 28).

Since the governing equations were nondimensionalized with respect to the external streams, some small arbitrary edge velocity was necessary. However, the velocity ratio u_{ζ}/u_e at the initial profile had to be large enough to reasonably represent the physical problem being studied but not so large that the accuracy on the low-velocity site would be limited by the peculiarities of the Von Mises transformation discussed previously. The values of u_{ζ}/u_e used in the initial profiles for the jets issuing into still air are listed in the following table:

Test case	Initial u_{ζ}/u_e
6	34.65
7	35.37
8	41.80
18	70.0
19	55.30

This length scale model was also used to compute test case 13, a two-dimensional jet in a moving stream.

Wakes.- Figure 3 shows the length scale model employed in wake flows. Again, a linear variation defined by the angle β is assumed to approximate the increased scale of turbulent motion when the boundary layers on the wake-generating body mix in the initial wake region. For region I in figure 3, the width $\bar{\delta}$ is given by

$$\bar{\delta}_I = (\text{Scaling factor})\left(\bar{y}_{.95} - \bar{y}_{\epsilon}\right) + \left(\bar{x} - \bar{x}_i\right)\tan \beta \quad (15)$$

where \bar{x}_i is the location of the start of region I which is usually the trailing edge of the body. Region I terminates when the two terms in equation (15) are of equal magnitude. The width $\bar{\delta}$ in region II is then given by

$$\bar{\delta}_{II} = 2(\text{Scaling factor})\left(\bar{y}_{.95} - \bar{y}_{\epsilon}\right) \quad (16)$$

The same scaling factor, 1.2, utilized in the jet flows downstream of the potential core was also used for wake flows.

Coaxial jets.- The model shown in figure 4(a) was employed for coaxial jet flows. The primary jet flow is assumed to mix with the initial boundary-layer flow in a region whose growth is characterized by mixing angles ϕ_1 , ϕ_2 , and ϕ_3 . In all calculations these angles were assumed to be equal. This model results in a radial distribution of $\bar{\delta}$, such as the one shown in figure 4(b), and features two overlapping scales of turbulent motion, $\bar{\delta}_{Outer}$ and $\bar{\delta}_{Inner}$, given by

$$\bar{\delta}_{Inner} = \bar{\delta}_{p,i} + 2\left(\bar{x} - \bar{x}_i\right)\tan \phi \quad (17)$$

$$\bar{\delta}_{Outer} = \left(\bar{y}_{.995} - \bar{r}_j\right) + \left(\bar{x} - \bar{x}_i\right)\tan \phi \quad (18)$$

where \bar{x}_i is measured from the exit plane of the primary jet nozzle. In the calculations, $\bar{\delta}$ is $\bar{\delta}_{Inner}$ for $\bar{y} < \bar{r}_p$ and $\bar{\delta}_{Outer}$ for $\bar{y} > \bar{r}_s$. Between \bar{r}_p and \bar{r}_s , $\bar{\delta}$ is found by a linear interpolation between $\bar{\delta}_{Inner}$ and $\bar{\delta}_{Outer}$. The nondimensional radii \bar{r}_p and \bar{r}_s are defined by

$$\bar{r}_p = \frac{1}{2}\left[\bar{r}_j + \left(\bar{x} - \bar{x}_i\right)\tan \phi\right] \quad (19)$$

and

$$\bar{r}_s = \begin{cases} \bar{r}_j + \frac{1}{2} \bar{\delta}_{s,i} & \text{for } \bar{x} \leq \bar{x}_c \\ \frac{1}{2} \left[\bar{r}_j + \bar{\delta}_{s,i} + (\bar{x} - \bar{x}_i) \tan \phi \right] & \text{for } \bar{x} > \bar{x}_c \end{cases} \quad (20)$$

where \bar{r}_j is the inner nozzle radius, \bar{x}_c is the location of the end of the core region, and $\bar{\delta}_{s,i}$ is the initial thickness of the external boundary layer. This length scale modeling allows (to zeroth order) for the orderly growth of the initial boundary layer (or shear layer) scales. Far downstream the more conventional approach of a single large scale for the entire flow is recovered.

A differential equation for the local length scale would obviously be better than the present approach just outlined. The purpose here is simply to point out that if the physics of scale development is taken into account, predictions are considerably improved. In the present approach, this scale development is handled in the simplest manner possible.

POSSIBLE INFLUENCE OF TRANSVERSE STATIC-PRESSURE GRADIENT ON TURBULENT FREE MIXING

The conventional approach to turbulent free mixing calculations (the approach used in the present paper) involves solving the boundary-layer equations with some turbulence closure model. On the basis of an order of magnitude analysis, the normal (or transverse) static-pressure gradient is assumed to be quite small in the basic boundary-layer equations. By assuming constant static pressure in the transverse direction, the solution of the normal momentum equation is unnecessary. Recent studies (refs. 29 and 30) indicate that this assumption of constant static pressure is not correct in boundary layers where there are large density changes across the layer. Changes in static pressure of 10 to 30 percent have been observed in nominally two-dimensional, high Mach number ($M > 6$) boundary layers.

The normal momentum equation for two-dimensional turbulent quasi-parallel shear flows takes the form

$$\frac{\partial p}{\partial y} = - \frac{\partial \left(\overline{\rho v^2} \right)}{\partial y} \quad (21)$$

where density fluctuations have been neglected in an order of magnitude analysis. Hinze (ref. 3) notes that for low-speed flows the normal static-pressure changes induced by the turbulence (from eq. (21)) were 2 orders of magnitude larger than the static-pressure changes induced by the mean flow. The basic question is whether or not the normal static-pressure gradient induced by the turbulence (eq. (21)) can become sufficiently large to affect the spreading rate and turbulence structure of a free turbulent mixing flow. The success of various calculation methods (turbulence closure models) in low-speed flows indicates that the influence is most likely negligible in these flows. However, large density changes would presumably increase the magnitude of the turbulence-induced normal static-pressure gradient (from eq. (21)); therefore, the answer to the basic question may well be that the spreading rate and turbulence structure are in fact affected where large density changes occur.

Estimates were made of the probable static-pressure change for an $M_1 = 5$ free shear layer obtained recently in the nozzle test apparatus at the Langley Research Center. (These data are discussed in paper 2 by Birch and Eggers.) By using the integrated form of equation (21) and estimates of $\overline{v'^2}$ from the subsonic shear layer of Liepmann and Laufer (ref. 12), the change in static pressure for this flow would be of the order of a 100-percent decrease near the maximum shear region. Obviously $\overline{v'^2}$ and perhaps the Reynolds stress must be lower than the normalized values of reference 12 for this $M_1 = 5$ case, since such a transverse static-pressure gradient would not be tolerated by the flow.

There are at least two possible mechanisms connected with a turbulence-induced $\partial p/\partial y$ which could affect the spreading rate of a free turbulent shear flow:

(1) Direct influence of turbulence-induced $\partial p/\partial y$ upon the normal mean velocity v and hence directly upon the spreading rate (refs. 31 and 32). A pressure gradient dp/dx is imposed within the shear flow.

(2) Indirect influence of turbulence-induced $\partial p/\partial y$ upon $\overline{v'^2}$ and $\overline{u'v'}$ by means of a turbulence field adjustment to decrease $\partial p/\partial y$ until a balance is achieved.

Obviously both of these mechanisms as well as others could be operating simultaneously. The important point is that as the density change across a turbulent free mixing region increases, the influence of the turbulence-induced $\partial p/\partial y$ may become increasingly more important, especially in determining the absolute physical dimensions of the flow field (i.e., the entrainment rate).

Transverse static-pressure data for free shear layers are available in references 32 to 34. For low-speed flows the data indicate a minimum pressure of the order of 2 percent near the inflection point in the velocity profile. The low-speed data of Lee (ref. 35) and Jones and Spencer (ref. 36) indicate small static-pressure changes (less than 1 per-

cent) for shear layers with $\frac{u_2}{u_1} = 0.35$ and 0.30 , respectively. Further data for the transverse static-pressure distribution in jets are available in references 31 and 37 and some data for wakes are found in reference 38. The available data do seem to indicate an increase of transverse static-pressure gradient with increasing Mach number across the shear layer.

It is interesting to note that the integrated form of equation (21) is

$$\left| \frac{\Delta p}{p_{\xi}} \right| \approx \left(\frac{\overline{\rho v'^2}}{p_{\xi}} \right)_{ip}$$

or

$$\left| \frac{\Delta p}{p_{\xi}} \right| \approx \frac{\overline{v'^2}}{u_{\xi}^2} \frac{\gamma_{\xi}}{\gamma_{ip}} M_{\xi}^2 \frac{R_{\xi}}{R_{ip}} \frac{T_{\xi}}{T_{ip}} \quad (22)$$

where the subscript ip indicates the inflection point in the shear-layer profile. Therefore, Mach number may well have an effect greater than simple density changes (caused by gas composition) upon possible changes in entrainment rate due to $\partial p / \partial y$.

The possibility that static-pressure variation may be responsible for the rather large changes in spreading rate with Mach number noted in connection with test case 2 in the present paper is entirely speculative at this point. There are several possible approaches that could be used to investigate this possibility. One such method would be to incorporate the complete normal momentum equation in a method such as Donaldson's (ref. 39) where $\overline{v'^2}$ is directly computed. If an equation for $\overline{v'^2}$ is lacking, it could be related to the Reynolds stress by some constant or function. Again, it would be necessary to solve the normal momentum equation (including the convective terms). The best method (i.e., most correct) of including the normal momentum equation would be a full field Navier-Stokes solution with turbulence terms included. However, if molecular diffusion of momentum is neglected in the normal momentum equation, a first-order solution may be obtained numerically by including the equation in a streamwise iteration loop with the usual boundary-layer equations.

There are, of course, other mechanisms which could also account for the disagreement between experiment and theory for case 2. These possibilities include the increased influence of $\overline{p'v'}$ and other terms in the second-order correlation equations. These

terms are usually negligible at low speeds but presumably become more important at high speeds. Currently there are no available models or data for these terms in high-speed flows which could be used to check this hypothesis.

RESULTS AND DISCUSSION

Solutions were obtained for all 17 of the primary test cases and for five of the seven optional cases. The two cases omitted were case 22, a hydrogen-air coaxial jet flow, and case 23, a subsonic compound coaxial air jet. These cases were omitted because of numerical and programming difficulties encountered rather than failure of the basic turbulence models being used.

During the investigation it was found that l/δ could be considered a function only of flow geometry. A value of 0.07 was used in all two-dimensional flows and 0.05 was used in all axisymmetric flows including the shear-layer region of jets.

In general, for constant density subsonic flows the turbulent Prandtl and Schmidt numbers were taken to be 1.0. For variable-density flows either 0.7 or 0.8 was used, with the Prandtl number assumed equal to the Schmidt number in all cases.

Two-Dimensional Shear Layers

Test case 1. - Two-dimensional subsonic constant-density free shear layers were computed for velocity ratios u_2/u_1 of 0.05, 0.2, 0.4, 0.6, and 0.8 by using "step" input profiles for velocity and temperature as previously described. Since the equations were normalized with respect to the secondary stream, a nominally zero value of u_2 was not possible in the present program; $\frac{u_2}{u_1} = 0.05$ was used in both test cases 1 and 2. The results from the computations of test case 1 are shown in figure 5. The spreading parameter σ is defined by the following relationship:

$$\sigma = \frac{1.855(X_B - X_A)}{Y_B - Y_A} \quad (23)$$

where Y_A and Y_B are the lateral distances between points at which $\frac{u - u_2}{u_1 - u_2}$ is 0.1 and 0.9 at longitudinal stations X_A and X_B , respectively. The spreading parameter σ is thus the reciprocal of the spreading rate of the shear layer.

Equation (12) was used to define the width $\bar{\delta}$, and l/δ was taken to be 0.07. By extrapolating the computed values of σ to the case where u_2/u_1 is zero, σ_0 was

found to be 11.4. This value was used to normalize the computed values of σ . As shown in figure 6, the results agree with the well-known relationship (from ref. 40)

$$\frac{\sigma_0}{\sigma} = \frac{u - u_2}{u_1 + u_2}$$

Test case 2.- Two-dimensional shear layers were computed for five values of M_1 to determine the effect of Mach number on the spreading rate (test case 2). The results are shown in figure 6 along with experimental data from references 12, 28, 31, 34, and 41 to 50 as well as the unpublished data recently obtained at the Langley Research Center at $M_1 = 5.0$. These shear-layer data have been adjudged the most reliable by Birch and Eggers in paper 2 of this compilation.

Equation (12) was used to define the width $\bar{\delta}$. With an l/δ of 0.07, only a slight increase in σ is predicted for increasing values of M_1 in striking contrast to much of the available data. At $M_1 = 5.0$, the effect of decreasing the mixing rate by lowering l/δ is shown. The cause underlying the inability of the mixing length model to predict the spreading rate of supersonic shear layers is perhaps directly related to the validity of the fundamental assumptions inherent in the boundary-layer approach to free mixing problems. One possible explanation is the existence of a transverse static-pressure gradient which could affect the turbulence spreading rate. The effect of such a pressure gradient was previously discussed in detail in this paper. There is also the possible influence of "low Reynolds number effects" as discussed by Birch and Eggers in paper 2. The data that may be influenced by such effects are indicated in figure 6. It should also be noted that the values of σ computed with $\frac{u_2}{u_1} = 0.05$ were scaled to correspond to $\frac{u_2}{u_1} = 0$ (using fig. 5).

Test case 3.- Test case 3 was designed to determine the effect of density ratio on the growth of fully developed two-dimensional shear layers. With $\frac{u_2}{u_1} = 0.2$, calculations were made for shear layers with density ratio ρ_1/ρ_2 of approximately 1/14, 2, 7, and 14. For all but the $\frac{\rho_1}{\rho_2} = \frac{1}{14}$ shear layer, the density difference was accounted for in the program by two methods: the subsonic mixing of gases with different molecular weights, and the mixing of two air streams with supersonic or hypersonic velocity in the primary stream. The $\frac{\rho_1}{\rho_2} = \frac{1}{14}$ shear layer was obtained by mixing hydrogen in the primary stream with air in the secondary stream. The $\frac{\rho_1}{\rho_2} = 2, 7, \text{ and } 14$ shear layers were the result of mixing hydrogen and helium, helium and air, and air and hydrogen; the corre-

sponding air into air equivalent density ratios were computed by using $M_1 = 2.24, 5.48,$ and $8.06,$ respectively. Turbulent Prandtl numbers of 0.7 and 0.8 were used for the dissimilar gas and supersonic flows, respectively; the turbulent Schmidt numbers were also 0.7 and $0.8,$ respectively. Appropriate input profiles of the type shown in figure 1 were used in each instance. The results, shown in figure 7, indicate that σ is a similar function of density differences irrespective of the mechanism producing that difference. However, it should be remembered that in test case 2 the supersonic results were greatly in error when compared with the data.

Test case 4.- Test case 4 considers the subsonic mixing of two streams initially developed on a symmetric airfoil with a 10° trailing edge. The coaxial jet length scale model was used for this calculation. A representative small angle of 8° (the value used in the slot injection studies of refs. 20 and 21) was used. The predicted profiles at two locations, $x = 12.7$ cm and $x = 76.2$ cm, are compared with Lee's experimental measurements (ref. 35) in figures 8(a) and 8(b), respectively. For this test case and test case 5, the computed profiles are matched with the experimental profiles at the point where $u = (u_1 - u_2)/2$ since the numerical calculation does not satisfy the proper boundary conditions (ref. 51). The predicted profile at $x = 12.7$ cm indicates only slightly more mixing than the experimental data. Much farther downstream at 76.2 cm the prediction indicates significantly more mixing. Better agreement could have been achieved by adjusting the angles $\phi_1, \phi_2,$ and ϕ_3 but such manipulation was beyond the intent of the current investigation. It should be noted that the streams mix with a fairly large initial angle (10°).

Test case 5.- The Hill and Page (ref. 50) supersonic ($M_1 = 2.09$) shear layer (test case 5) was computed with $l/\delta = 0.07,$ where $\bar{\delta}$ was defined by equation (12). Computed profiles at two stations are shown in figure 9. The effect of the different boundary conditions used in the computations is evident on the low-velocity side of the shear layer. The data were obtained in a cavity-type flow and may be influenced by the "low Reynolds number effects." Both calculated profiles indicate more rapid mixing than the experimental data, which is the expected behavior from the results of test case 2. (See section entitled "Possible Influence of Transverse Static-Pressure Gradient on Turbulent Free Mixing.")

Jets Issuing Into Still Air

For all flows of this type the length scale model of figure 2 was employed. An l/δ of 0.05 was used in all three regions of the axisymmetric jets including region I. The value of l/δ should actually be varied from 0.07 at the nozzle exit where the shear layer is thin and essentially two-dimensional to 0.05 at the end of the core where the flow is fully axisymmetric. Hence, for flows with relatively short potential cores (e.g., test cases 6 and 8) the use of a single value lower than the average value through the core

results in less mixing and hence too long a potential case. The present model predicted the decay of the center-line velocity remarkably well by using an angle ϕ of 8° .

Test case 6.- Figure 10 shows the results of the computation of the Maestrello and McDaid subsonic jet (ref. 52). The potential core is longer than indicated by the experimental data but the decay rate of the center-line velocity in regions II and III is well predicted. Test case 6 is an example of a jet for which l/δ must have a value near 0.07 in the shear-layer region to correctly predict the core length.

Test case 7.- For the Eggers Mach 2.22 jet (ref. 49), the potential core length is well predicted, but the agreement with the center-line velocity decay curve using $\phi = 8^\circ$ is not as good as the corresponding comparison in the previous subsonic jet flow in test case 6. The prediction for test case 7 is shown in figure 11(a) with a $\phi = 89^\circ$ calculation which corresponds to an immediate jump in length scale at the end of the core to the region III value. This represents the usual method of applying the mixing length model to jet flows (e.g., Harsha, ref. 19). Obviously the prediction of the center-line velocity decay as the far field is approached is significantly improved by using a "length scale equation" between the near field and far field. A prediction with $\phi = 0^\circ$ is also shown. Velocity profiles at three locations are shown in figures 11(b) and 11(c). These results indicate that the correct profile is obtained when the center-line value is correctly predicted.

Test case 8.- A value of l/δ of 0.05 and mixing angle of 8° were used to predict the high-temperature subsonic data of Heck (ref. 53). The center-line distributions of velocity and temperature for test case 8 are given in figures 12(a) and 12(b), respectively. As shown in these figures, the velocity potential core length is again incorrect although the velocity decay rate outside the core is well matched. A turbulent Prandtl number of 0.7 predicts the temperature decay rate correctly.

Test case 18.- The fully developed axisymmetric jet data of Wagnanski and Fiedler (ref. 28) provided a test of the far field length scale model in a subsonic flow (test case 18). Starting with the given similarity profile at $x/D = 60$, a location in the self-preserving region, the solution was obtained with $l/\delta = 0.05$. With an initial velocity ratio u_t/u_e of 70, the computed spreading rate of the jet was found to be linear and in excellent agreement with the data. Figure 13(a) shows the center-line velocity prediction over the range of the data. The similarity of the data was retained in the calculations as shown in figure 13(b) where x_{v0} indicates the streamwise distance from the virtual origin of the jet. Equation (14) was used to define δ .

Test case 19.- Test case 19 is a supersonic high-temperature jet (ref. 53) similar to the subsonic jet of test case 8. The turbulent Prandtl number was assumed to be 0.7 and $l/\delta = 0.05$ and $\phi = 8^\circ$. Figure 14(a) shows that the predicted potential core is too long; however, the correct velocity decay rate is predicted as the far field is approached.

Figure 14(b) indicates that similar conclusions apply to the center-line temperature distribution. If the core length problem could be remedied for compressible shear-layer mixing, the center-line variation would then probably be correctly predicted for the entire flow field.

In all the compressible jet cases it should be noted that the near field (where the present calculations give least accurate agreement with data) is the only region where large density gradients occur. It is speculated that the mechanism responsible for the disagreement in this region is the same mechanism operative in the supersonic free shear layers. In the present paper it is suggested that this mechanism is related to turbulence-induced static-pressure gradients. Other possible mechanisms operable in this region are the "low Reynolds number effect" discussed by Birch and Eggers in paper 2 and the l/δ adjustment from two-dimensional to axisymmetric.

Plane Jet in a Moving Stream

Test case 13.- The length scale model shown in figure 2 was used to predict subsonic test case 13. No initial profile data were available other than the experimentally determined momentum thickness and u_j/u_e . A step velocity profile was selected so that u_j/u_e was matched. Value of l/δ of 0.07 and a mixing angle of 8° gave an excellent prediction of the center-line velocity distribution as shown in figure 15. Since the external stream had a constant nonzero velocity, the experimental velocity ratio u_c/u_e could be accurately represented numerically, unlike the previously discussed jets issuing into still air.

Coaxial Jet Flows

The length scale model shown in figure 4 was used for all flows of this type. A value of l/δ of 0.05 was used in regions I and II. All solutions were started at the nozzle exit with the initial boundary-layer profiles. For the AEDC experimental data (test cases 10, 20, and 21) these profiles were approximated by using the estimates of boundary-layer thicknesses given in reference 54. The mixing angles ϕ_1 , ϕ_2 , and ϕ_3 were taken to be equal in all cases.

Test case 9.- Test case 9 represents the data of Forstall and Shapiro (ref. 55). The suggested initial profile, which was adjusted to account for probable pitot probe positioning errors, was used to start the solution. The results of the computation using $l/\delta = 0.05$ and all mixing angles equal to 8° are shown in figure 16. The experimental center-line velocity decay in region II is well predicted by using angles of 8° although the potential core length is unpredicted. However, it should be noted that the core length is a function of ϕ_3 for a given l/δ . As discussed previously, a larger average l/δ is needed in the core.

Test case 10.- Figure 17 shows the results of applying the coaxial jet length scale model to the subsonic hydrogen-air data of Chriss (ref. 56). Both the center-line velocity and center-line hydrogen concentration variations for test case 10 are well predicted with $l/\delta = 0.05$ and mixing angles of 8° .

Test case 11.- Figure 18 shows the computational results for test case 11 which represents an inner subsonic air jet mixing with an outer Mach 1.30 air jet studied by Eggers and Torrence (ref. 57). Mixing angles of 2° gave better predictions of the center-line velocity variation than did angles of 8° . However, neither calculation predicted as large a drop in center-line velocity as the data indicate and neither calculation correctly predicted the rate of velocity increase as the far field is approached.

Test case 12.- Good prediction of the center-line velocity decrease for the hydrogen-air data of Eggers (ref. 58) was obtained for test case 12 with $l/\delta = 0.05$ and mixing angles of 8° even though this choice of angle resulted in an underprediction of the potential core length. The center-line velocity distribution is shown in figure 19(a). The same prediction trend is also observed in the center-line hydrogen concentration variation as shown in figure 19(b). The turbulent Schmidt and Prandtl numbers were both 0.8.

Test case 20.- Test case 20 represents the mixing of subsonic coaxial jets as measured by Chriss and Paulk (ref. 54). The best overall prediction with the coaxial length scale model was achieved with mixing angles of 6° as shown in figure 20. The calculations with angles of 6° and 8° are shown for comparison; however, as discussed previously, l/δ should actually have had a larger average value through the core region.

Test case 21.- As shown in figure 21(a) the coaxial model again predicted the correct center-line velocity decay rate for the subsonic hydrogen-air data of Chriss (ref. 56). However, a value of l/δ of 0.05 gave an overprediction of the potential core length for a mixing angle of 8° . An l/δ of 0.07 with all angles ϕ (i.e., ϕ_1, ϕ_2, ϕ_3) equal to 8° gives a better core length prediction. The concentration profile prediction for test case 21 is given in figure 21(b).

Wake Flows

The length scale model shown in figure 3 was used in computing all wake flows. In addition, the effect of including the second-derivative term (eq. (5)) was investigated for some of these wakes.

Test case 14.- The predicted center-line velocity distribution is shown in figure 22 for the two-dimensional wake data (test case 14) of Chevray and Kovasznay (ref. 59). By using a value of l/δ of 0.07 and a mixing angle β of 8° , a reasonably accurate overall prediction is obtained. As expected, addition of the second-derivative term (with $\frac{l_{sd}}{\delta} = \frac{l}{\delta}$)

results in an increase in the mixing rate, the increase giving a more accurate velocity rise in the near wake region while overpredicting the data as the far field is approached. A calculation with $\phi = 89^\circ$, which corresponds to using no linear variation in length scale downstream of the body, is shown to demonstrate the improved prediction in the near wake region with the present linear variation. The effect of the angle disappears as the asymptotic region is approached. A calculation with $\beta = 4^\circ$ and no second-derivative term is also shown for comparison.

The deviation between prediction and experiment in the far field is emphasized when the data is plotted in terms of $1/w_\zeta^2$ where w_ζ is the center-line velocity defect.

Test case 15.- Computations of Chevray's axisymmetric wake (ref. 60) with $\frac{l}{\delta} = 0.05$ and $\beta = 8^\circ$ are shown in figure 23. The initial rapid increase of the center-line velocity (due in part to the pressure gradient just behind the body) is not predicted even when the second-derivative term (with $\frac{l_{sd}}{\delta} = \frac{l}{\delta}$) is included. The second-derivative model, however, gives better downstream agreement than the basic model. Test case 15 is an example of a flow in which the value of β probably should be high initially and lowered to 8° a few diameters downstream (as is done automatically by the method of ref. 20), but such optimization was beyond the present intent.

Test case 16.- The asymptotic region of the plane supersonic wake of Demetriades (ref. 61) is well predicted with $\frac{l}{\delta} = 0.07$ and $\beta = 8^\circ$. (See fig. 24.) The second derivative increases the mixing rate only slightly for test case 16.

Test case 17.- The supersonic ($M = 3.0$) axisymmetric wake data of Demetriades (ref. 62) is underpredicted for test case 17 with $\frac{l}{\delta} = 0.05$ and $\beta = 8^\circ$ even though the second-derivative term is included. (See fig. 25.) The calculation was started at $\frac{x}{D} = 17$, a location actually near the end of the transition region; hence these data may be influenced by the "low Reynolds number effects." Assuming turbulent flow at $\frac{x}{D} = 17$ results in an underprediction of the data in the turbulent region ($\frac{x}{D} > 20$).

Test case 24.- The two-dimensional supersonic wake data of Demetriades (ref. 63) include data in the transition region ($602.9 \leq \frac{x}{D} \leq 938.4$). The wake-generating wedge was heated so that transition would occur far downstream of the model. The calculation for test case 24 was started in the laminar region at $\frac{x}{D} = 183.7$. In reference 64 Demetriades

gives the experimental streamwise distribution of the intermittency factor on the wake center line for the corresponding unheated flow. This distribution was used to compute through the given region of transitional flow. Such an approach had previously been employed by Harris (ref. 65) who used the streamwise intermittency function of Dhawan and Narasimha (ref. 66) in the computation of compressible boundary layers. The results shown in figure 26 indicate that the data were slightly underpredicted in the laminar and transitional regions with improved agreement in the fully turbulent region. A wake flow mixing angle of 8° was used.

CONCLUDING REMARKS

Prandtl's mixing length model has been applied in a consistent manner to compute the wide range of free turbulent mixing flows selected as test cases in this compilation. On the basis of these computations, the following concluding remarks can be made.

The mixing length constant l/δ was found to be lower in axisymmetric flows than in planar flows. With $l/\delta = 0.05$ in axisymmetric flows and 0.07 in two-dimensional flows, the calculations compare very favorably with the data for jets downstream of the core, wake flows, and low-speed shear layers.

For the mixing of flows with differing or developing turbulent length scales (such as near field to far field transition region in a jet and wake flows developing from boundary layers), some method of correctly determining the local length scale should be used. In the present paper, a linear algebraic function based on modeling the physical spreading of the turbulence was used. Perhaps a more satisfactory approach would be the use of one of the various "two-equation" turbulence models of Spalding's group (paper 11 of this compilation) where a differential length scale equation is solved.

The mixing length model was unable to successfully compute the spreading rates of free shear layers with large sustained density differences. This inability is tentatively ascribed to the assumption of constant static pressure in the transverse direction (the conventional quasi-parallel flow assumption). Therefore, a successful calculation method for this class of flows (free turbulent mixing flows with sustained large density changes or differences) may necessitate including equations for the mean normal momentum and v'^2 .

As discussed by Birch and Eggers in paper 2 of this compilation, there seems to be an important "low Reynolds number effect" in some of the available data. However, further analysis of the data is needed before this effect can be incorporated into prediction methods.

REFERENCES

1. Prandtl, L.: Bericht über Untersuchungen zur ausgebildeten Turbulenz. Z. Angew. Math. Mech., Bd. 5, Heft 2, Apr. 1925, pp. 136-139. (Available in English translation as NACA TM 1231, 1949.)
2. Prandtl, L.: Ueber die ausgebildete Turbulenz. Lecture presented at International Congress for Applied Mechanics (Zurich), Sept. 1926. (Available in English translation as NACA TM 435, 1927.)
3. Hinze, J. O.: Turbulence. McGraw-Hill Book Co., Inc., 1959.
4. Schlichting, Hermann (J. Kestin, transl.): Boundary-Layer Theory. Sixth ed., McGraw-Hill Book Co., 1968.
5. Pletcher, Richard H.: On a Finite-Difference Solution for the Constant-Property Turbulent Boundary Layer. AIAA J., vol. 7, no. 2, Feb. 1969, pp. 305-311.
6. Ng, K. H.; Patankar, S. V.; and Spalding, D. B.: The Hydrodynamic Turbulent Boundary Layer on a Smooth Wall, Calculated by a Finite-Difference Method. Computation of Turbulent Boundary Layers - 1968 AFOSR-IFP-Stanford Conference, Vol. I, S. J. Kline, M. V. Morkovin, G. Sovran, and D. J. Cockrell, eds., Stanford Univ., c.1969, pp. 356-365.
7. Patankar, S. V.; and Spalding, D. B.: Heat and Mass Transfer in Boundary Layers. Second ed., Int. Textbook Co. Ltd. (London), c.1970.
8. Adams, John C., Jr.: Eddy Viscosity-Intermittency Factor Approach to Numerical Calculation of Transitional Heating on Sharp Cones in Hypersonic Flow. AEDC-TR-70-210, U.S. Air Force, Nov. 1970.
9. Bushnell, Dennis M.; and Beckwith, Ivan E.: Calculation of Nonequilibrium Hypersonic Turbulent Boundary Layers and Comparisons With Experimental Data. AIAA J., vol. 8, no. 8, Aug. 1970, pp. 1462-1469.
10. Kuethe, Arnold M.: Investigations of the Turbulent Mixing Regions Formed by Jets. J. Appl. Mech., vol. 2, no. 3, Sept. 1935, pp. A-87 - A-95.
11. Squire, H. B.; and Truncer, J.: Round Jets in a General Stream. R. & M. No. 1974, Brit. A.R.C., 1944.
12. Liepmann, Hans Wolfgang; and Laufer, John: Investigations of Free Turbulent Mixing. NACA TN 1257, 1947.
13. Alexander, Lloyd G.; Baron, Thomas; and Comings, Edward W.: Transport of Momentum, Mass, and Heat in Turbulent Jets. Bull. Ser. No. 413, Univ. of Illinois, May 1953.

14. Batchelor, G. K.: Note on Free Turbulent Flows, With Special Reference to the Two-Dimensional Wake. *J. Aeronaut. Sci.*, vol. 17, no. 7, July 1950, pp. 441-445.
15. Rodi, W.; and Spalding, D. B.: A Two-Parameter Model of Turbulence, and Its Application to Free Jets. *Wärme- und Stoffübertragung*, vol. 3, no. 2, 1970, pp. 85-95.
16. Prandtl, L.: Bemerkungen zur Theorie der freien Turbulenz. *Z. Angew. Math. & Mech.*, Bd. 22, Heft 5, Oct. 1942, pp. 241-243.
17. Elassar, R. J.; and Pandolfini, P. P.: An Examination of Eddy Viscosity Models for Turbulent Free Shear Flows. Paper No. 71-FE-17, Amer. Soc. Mech. Eng., May 9-12, 1971.
18. Wagner, Richard D.: Measured and Calculated Mean-Flow Properties of a Two-Dimensional, Hypersonic, Turbulent Wake. NASA TN D-6927, 1972.
19. Harsha, Philip Thomas: Free Turbulent Mixing: A Critical Evaluation of Theory and Experiment. AEDC-TR-71-36, U.S. Air Force, Feb. 1971. (Available from DDC as AD 718 956.)
20. Beckwith, Ivan E.; and Bushnell, Dennis M.: Calculation by a Finite-Difference Method of Supersonic Turbulent Boundary Layers With Tangential Slot Injection. NASA TN D-6221, 1971.
21. Bushnell, Dennis M.: Calculation of Relaxing Turbulent Boundary Layers Downstream of Tangential Slot Injection. *J. Spacecraft & Rockets*, vol. 8, no. 5, May 1971, pp. 550-551.
22. Spalding, Dudley Brian: A Two-Equation Model of Turbulence. *VDI-Forsch.*, Heft 549, 1972, pp. 5-16.
23. Bushnell, Dennis M.; and Morris, Dana J.: Shear-Stress, Eddy-Viscosity, and Mixing-Length Distributions in Hypersonic Turbulent Boundary Layers. NASA TM X-2310, 1971.
24. Sinha, Ram; Fox, Herbert; and Weinberger, Lawrence: An Implicit Finite Difference Solution for Jet and Wake Problems. Pt. I: Analysis and Test Cases. ARL 70-0025, U.S. Air Force, Feb. 1970. (Available from DDC as AD 707 865.)
25. Sinha, Ram; Fox, Herbert; and Weinberger, Lawrence: An Implicit Finite Difference Solution for Jet and Wake Problems. Pt. II: Program Manual. ARL 70-0024, U.S. Air Force, Feb. 1970. (Available from DDC as AD 707 866.)
26. Hopf, H.; and Fortune, O.: Diffusion Controlled Combustion for Scramjet Application. Pt. II - Programmer's Manual. Tech. Rep. 569 (Contract No. NAS 1-5117), Gen. Appl. Sci. Lab., Inc., Dec. 1965.

27. Halleen, R. M.: A Literature Review on Subsonic Free Turbulent Shear Flow. AFOSR-TN-5444, U.S. Air Force, Apr. 1964. (Available from DDC as AD 606 758.)
28. Wagnanski, I.; and Fiedler, H.: Some Measurements in the Self-Preserving Jet. J. Fluid Mech., vol. 38, pt. 3, Sept. 18, 1969, pp. 577-612.
29. Laderman, A. J.; and Demetriades, A.: Measurements of the Mean and Turbulent Flow in a Cooled-Wall Boundary Layer at Mach 9.37. AIAA Paper No. 72-73, Jan. 1972.
30. Fischer, M. C.; Maddalon, D. V.; Weinstein, L. M.; and Wagner, R. D., Jr.: Boundary-Layer Pitot and Hot-Wire Surveys at $M_\infty \approx 20$. AIAA J., vol. 9, no. 5, May 1971, pp. 826-834.
31. Johannesen, N. H.: Further Results on the Mixing of Free Axially-Symmetrical Jets of Mach Number 1.40. R. & M. No. 3292, Brit. A.R.C., 1962.
32. Warren, Walter R., Jr.: The Static Pressure Variation in Compressible Free Jets. J. Aeronaut. Sci., vol. 22, no. 3, Mar. 1955, pp. 205-207.
33. Pitkin, Edward T.; and Glassman, Irvin: Experimental Mixing Profiles of a Mach 2.6 Free Jet. J. Aerosp. Sci., vol. 25, no. 12, Dec. 1958, pp. 791-793.
34. Maydew, R. C.; and Reed, J. F.: Turbulent Mixing of Axisymmetric Compressible Jets (in the Half-Jet Region) With Quiescent Air. SC-4764(RR), Sandia Corp. (Albuquerque, N. Mex.), Mar. 1963.
35. Lee, Shen Ching: A Study of the Two-Dimensional Free Turbulent Mixing Between Converging Streams With Initial Boundary Layers. Ph. D. Diss., Univ. of Washington, 1966.
36. Jones, Barclay G.; and Spencer, Bruce W.: A Study of the Local Pressure Field in Turbulent Shear Flow and Its Relation to Aerodynamic Noise Generation. SR-2 (Grant No. NASA NGR 14-005-149), Univ. of Illinois, Jan. 31, 1971. (Available as NASA CR-119339.)
37. Miller, David R.; and Comings, Edward W.: Static Pressure Distribution in the Free Turbulent Jet. J. Fluid Mech., vol. 3, pt. 1, Oct. 1957, pp. 1-16.
38. Schetz, Joseph A.: Some Studies of the Turbulent Wake Problem. Astronaut. Acta, vol. 16, no. 2, Feb. 1971, pp. 107-117.
39. Donaldson, Coleman duP.: Calculation of Turbulent Shear Flows for Atmospheric and Vortex Motions. AIAA J., vol. 10, no. 1, Jan. 1972, pp. 4-12.
40. Sabin, C. M.: An Analytical and Experimental Study of the Plane, Incompressible, Turbulent Free Shear Layer With Arbitrary Velocity Ratio and Pressure Gradient. AFOSR-TN-5443, U.S. Air Force, Oct. 1963. (Available from DDC as AD 430 120.)

41. Tollmien, Walter: Berechnung turbulenter Ausbreitungsvorgänge. *Z. Angew. Math. Mech.*, Bd. 6, Heft 6, Dec. 1926, pp. 468-478. (Available in English translation as NACA TM 1085, 1945.)
42. Cordes, G.: Untersuchungen zur statischen Druckmessung in turbulenter Strömung. *Ing.-Arch.*, Bd. VIII, Heft 4, Aug. 1937, pp. 245-270.
43. Reichardt, Hans: Gesetzmässigkeiten der freien Turbulenz. *VDI-Forschungsh.* 414, 1942.
44. Gooderum, Paul B.; Wood, George P.; and Brevoort, Maurice J.: Investigation With an Interferometer of the Turbulent Mixing of a Free Supersonic Jet. NACA Rep. 963, 1950. (Supersedes NACA TN 1857.)
45. Bershader, D.; and Pai, S. I.: On Turbulent Jet Mixing in Two-Dimensional Supersonic Flow. *J. Appl. Phys.*, vol. 21, no. 6, June 1950, p. 616.
46. Crane, L. J.: The Laminar and Turbulent Mixing of Jets of Compressible Fluid. Pt. II - The Mixing of Two Semi-Infinite Streams. *J. Fluid Mech.*, vol. 3, pt. I, Oct. 1957, pp. 81-92.
47. Rhudy, J. P.; and Magnan, J. D., Jr.: Turbulent Cavity Flow Investigation at Mach Numbers 4 and 8. AEDC-TR-66-73, U.S. Air Force, June 1966. (Available from DDC as AD 483 748.)
48. Sirieix, M.; and Solognac, J. L.: Contribution a l'Etude Experimentale de la Couche de Melange Turbulent Isobare d'un Ecoulement Supersonique. *Separated Flows*, Pt. I, AGARD CP No. 4, May 1966, pp. 241-270.
49. Eggers, James M.: Velocity Profiles and Eddy Viscosity Distributions Downstream of a Mach 2.22 Nozzle Exhausting to Quiescent Air. NASA TN D-3601, 1966.
50. Hill, W. G., Jr.; and Page, R. H.: Initial Development of Turbulent, Compressible, Free Shear Layers. *Trans. ASME, Ser. D: J. Basic Eng.*, vol. 91, no. 1, Mar. 1969, pp. 67-73.
51. Lock, R. C.: The Velocity Distribution in the Laminar Boundary Layer Between Parallel Streams. *Quart. J. Mech. & Appl. Math.*, vol. IV, pt. 1, 1951, pp. 42-63.
52. Maestrello, L.; and McDaid, E.: Acoustic Characteristics of a High-Subsonic Jet. *AIAA J.*, vol. 9, no. 6, June 1971, pp. 1058-1066.
53. Heck, P. H.: Jet Plume Characteristics of 72-Tube and 72-Hole Primary Suppressor Nozzles. T.M. No. 69-457 (FAA Contract FA-SS-67-7), Flight Propulsion Div., Gen. Elec. Co., July 1969.

54. Chriss, D. E.; and Paulk, R. A.: An Experimental Investigation of Subsonic Coaxial Free Turbulent Mixing. AEDC-TR-71-236, AFOSR-72-0237TR, U.S. Air Force, Feb. 1972. (Available from DDC as AD 737 098.)
55. Forstall, Walton, Jr.; and Shapiro, Ascher H.: Momentum and Mass Transfer in Coaxial Gas Jets. J. Appl. Mech., vol. 17, no. 4, Dec. 1950, pp. 399-408.
56. Chriss, D. E.: Experimental Study of the Turbulent Mixing of Subsonic Axisymmetric Gas Streams. AEDC-TR-68-133, U.S. Air Force, Aug. 1968. (Available from DDC as AD 672 975.)
57. Eggers, James M.; and Torrence, Marvin G.: An Experimental Investigation of the Mixing of Compressible-Air Jets in a Coaxial Configuration. NASA TN D-5315, 1969.
58. Eggers, James M.: Turbulent Mixing of Coaxial Compressible Hydrogen-Air Jets. NASA TN D-6487, 1971.
59. Chevray, René; and Kovasznay, Leslie S. G.: Turbulence Measurements in the Wake of a Thin Flat Plate. AIAA J., vol. 7, no. 8, Aug. 1969, pp. 1641-1643.
60. Chevray, R.: The Turbulent Wake of a Body of Revolution. Trans. ASME, Ser. D: J. Basic Eng., vol. 90, no. 2, June 1968, pp. 275-284.
61. Demetriades, Anthony: Turbulent Mean-Flow Measurements in a Two-Dimensional Supersonic Wake. Phys. Fluids, vol. 12, no. 1, Jan. 1969, pp. 24-32.
62. Demetriades, Anthony: Mean-Flow Measurements in an Axisymmetric Compressible Turbulent Wake. AIAA J., vol. 6, no. 3, Mar. 1968, pp. 432-439.
63. Demetriades, Anthony: Observations on the Transition Process of Two-Dimensional Supersonic Wakes. AIAA J., vol. 9, no. 11, Nov. 1971, pp. 2128-2134.
64. Demetriades, Anthony: Observations on the Transition Process of Two-Dimensional Supersonic Wakes. AIAA Paper No. 70-793, June-July 1970.
65. Harris, Julius E.: Numerical Solution of the Equations for Compressible Laminar, Transitional, and Turbulent Boundary Layers and Comparisons With Experimental Data. NASA TR R-368, 1971.
66. Dhawan, S.; and Narasimha, R.: Some Properties of Boundary Layer Flow During the Transition From Laminar to Turbulent Motion. J. Fluid Mech., vol. 3, pt. 4, Jan. 1958, pp. 418-436.

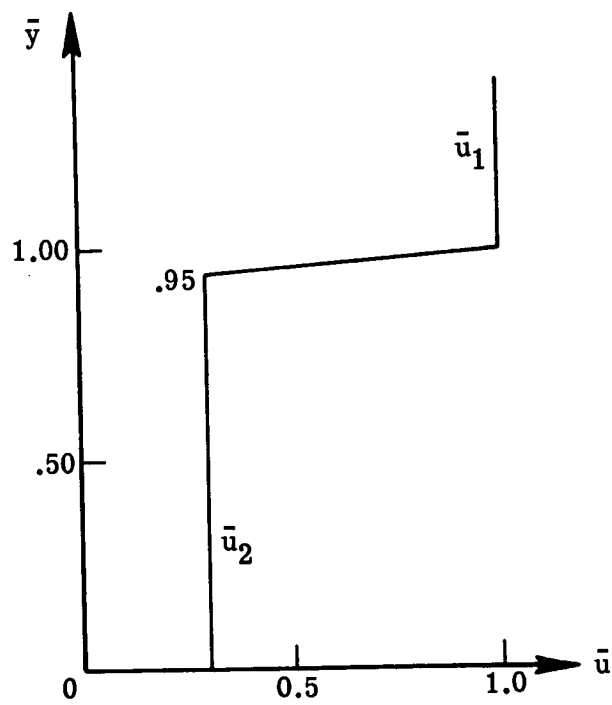


Figure 1.- Initial velocity profile used in two-dimensional shear-layer calculations. Test cases 1 to 3.

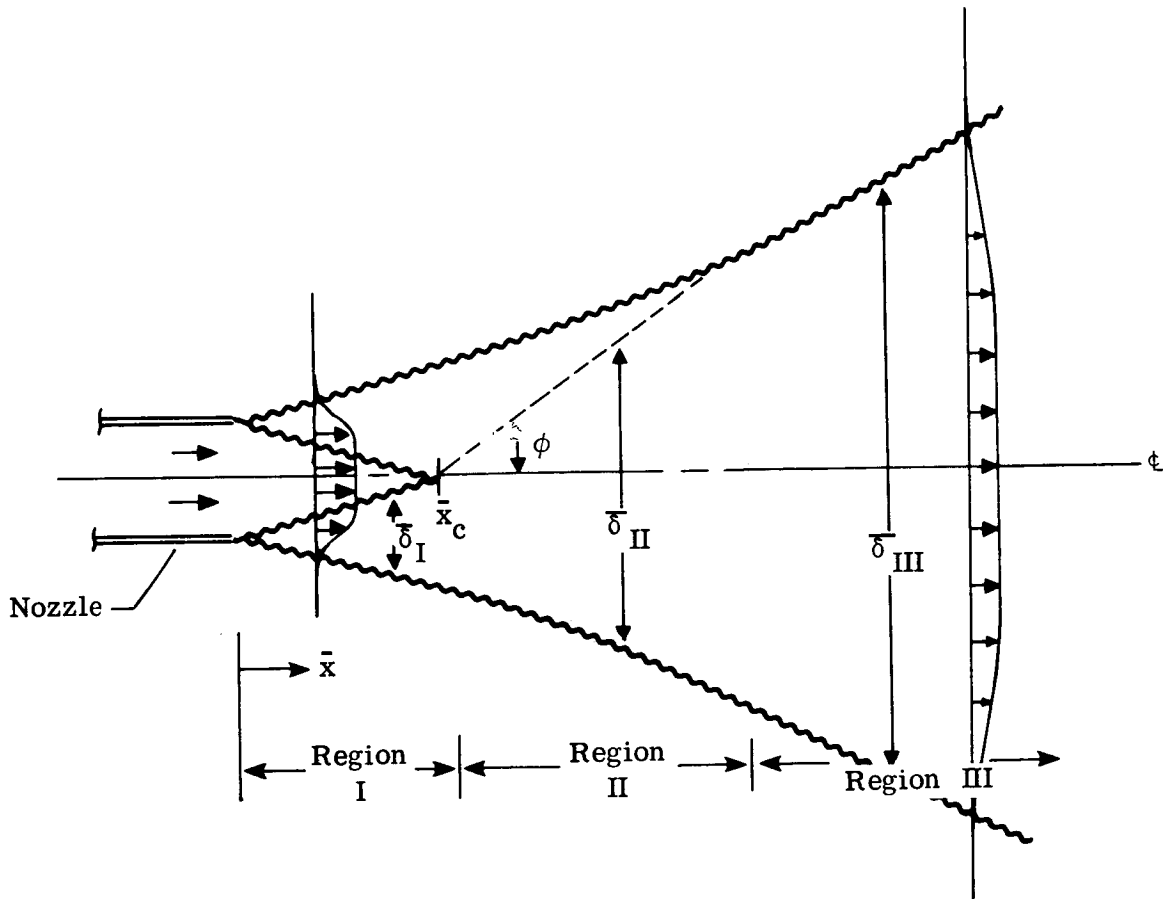


Figure 2.- Definition of mixing region width for jets issuing into still air.

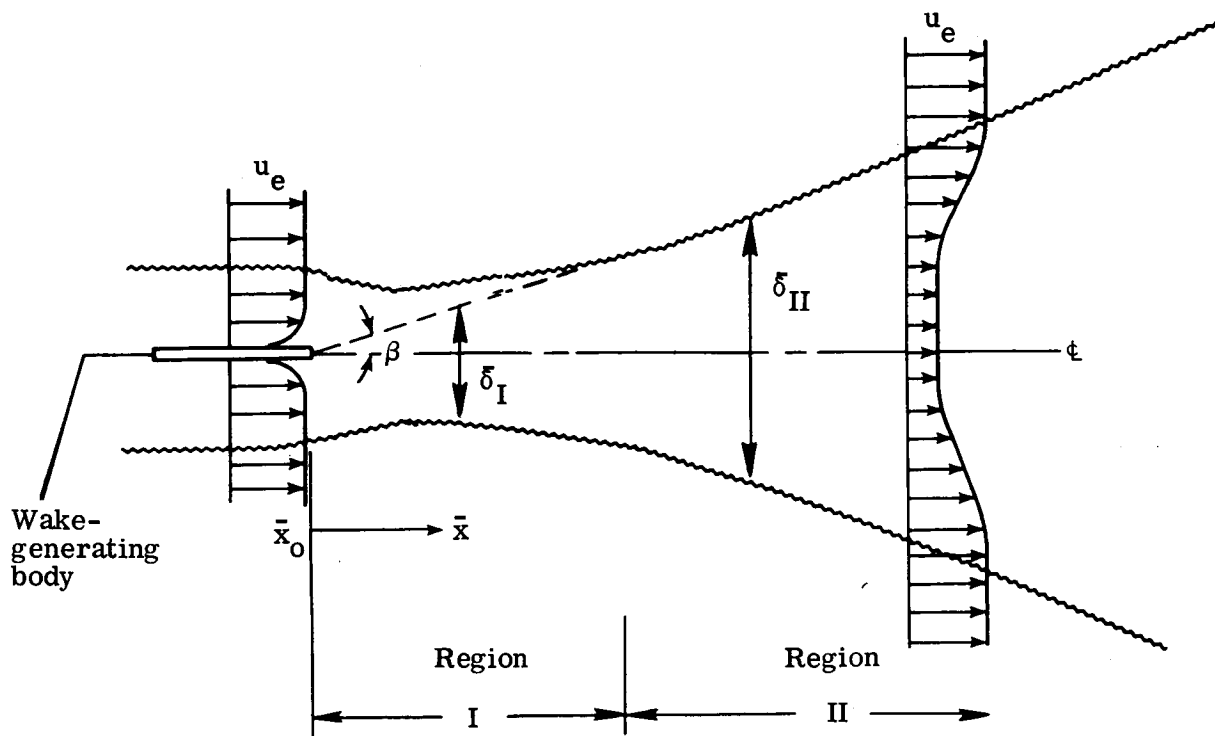
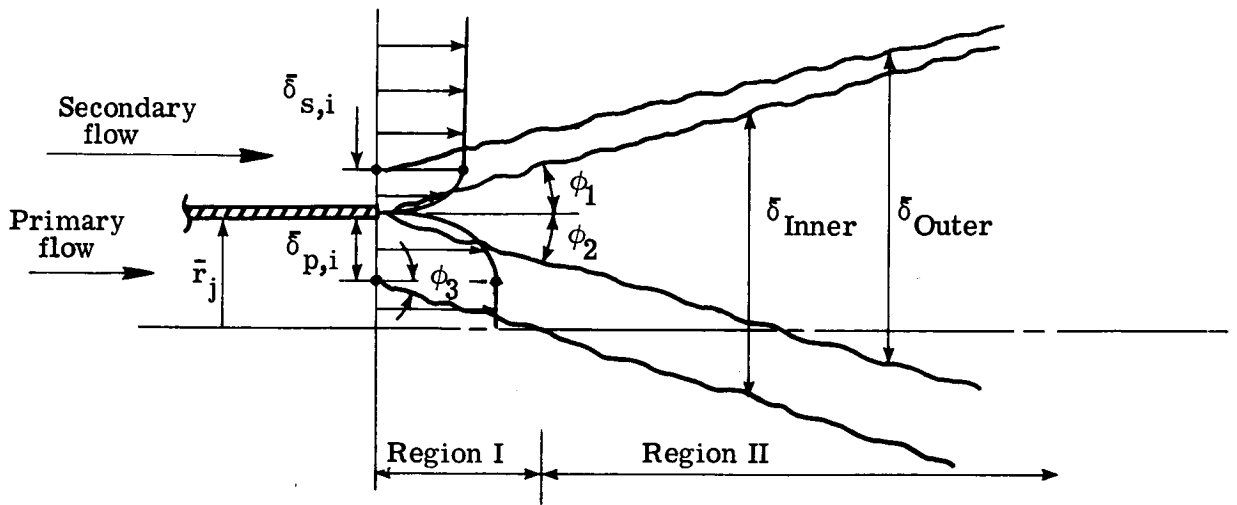
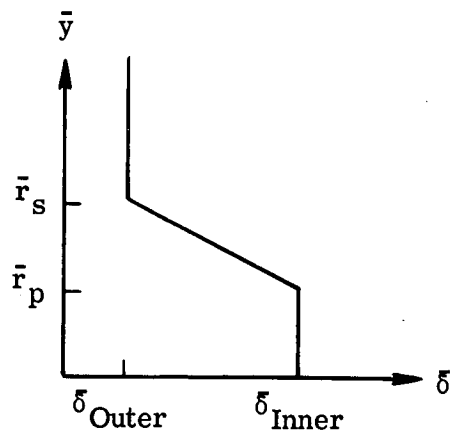


Figure 3.- Definition of mixing region width for wake flows.



(a) Sketch of idealized flow field.



(b) Variation of $\bar{\delta}$ with \bar{y} .

Figure 4.- Definition of mixing region width for coaxial jet flows.

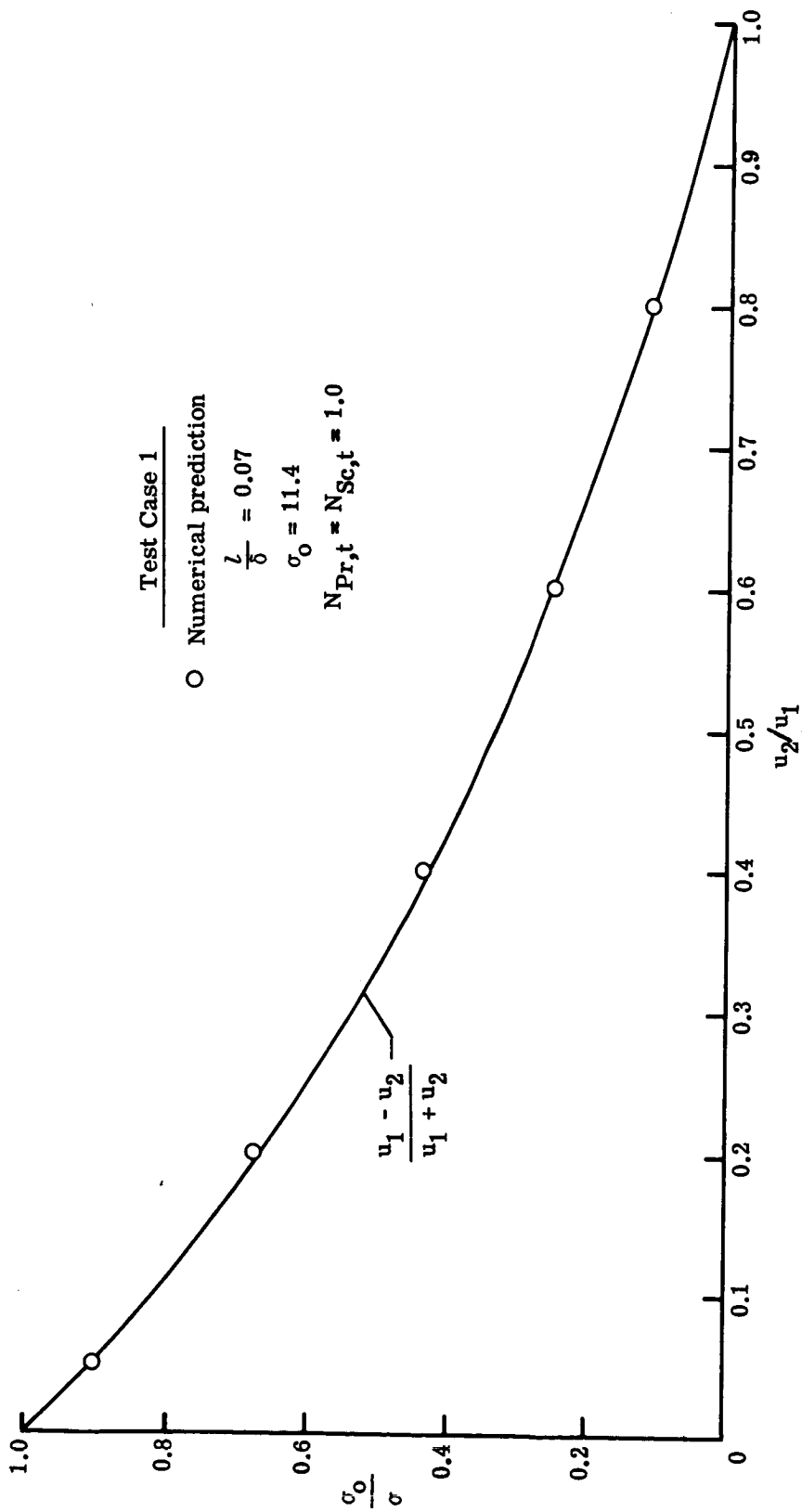
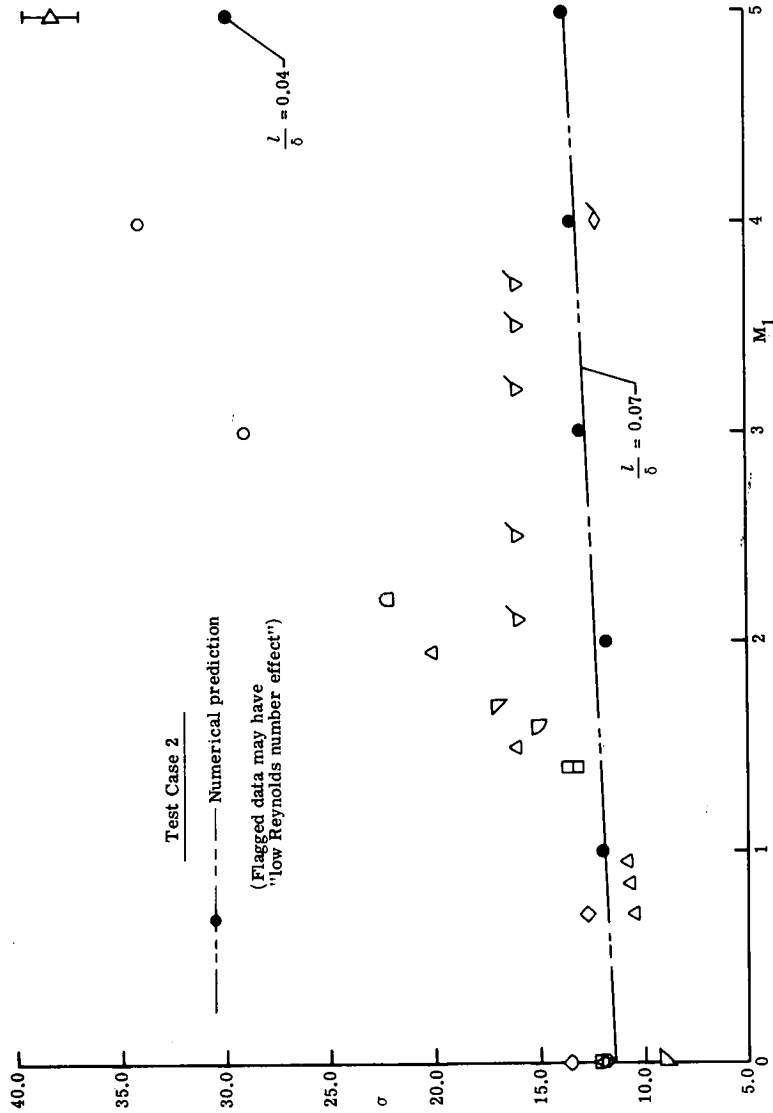


Figure 5.- Variation of spreading parameter with velocity ratio for two-dimensional subsonic constant-density free shear layers. Test case 1.



Symbol	Author	Date	Reference
◇	Tollmien	1926	41
◇	Cordes	1937	42
◇	Reichardt	1942	43
◇	Liepmann and Laufer	1947	12
◇	Goederum, Wood, and Brevoort	1949	44
◇	Bershadner and Pal	1950	45
◇	Crane	1957	46
◇	Johannesen	1959	31
◇	Maydew and Reed	1963	34
◇	Rhudy and Magnan	1966	47
◇	Sirteix and Solignac	1966	48
◇	Eggers	1966	49
◇	Hill and Page	1969	50
◇	Wyganski and Fiedler	1969	28
◇	Morrisette and Birch	1972	Unpublished

Figure 6.- Effect of Mach number on spreading parameter for two-dimensional free shear layers. Test case 2.

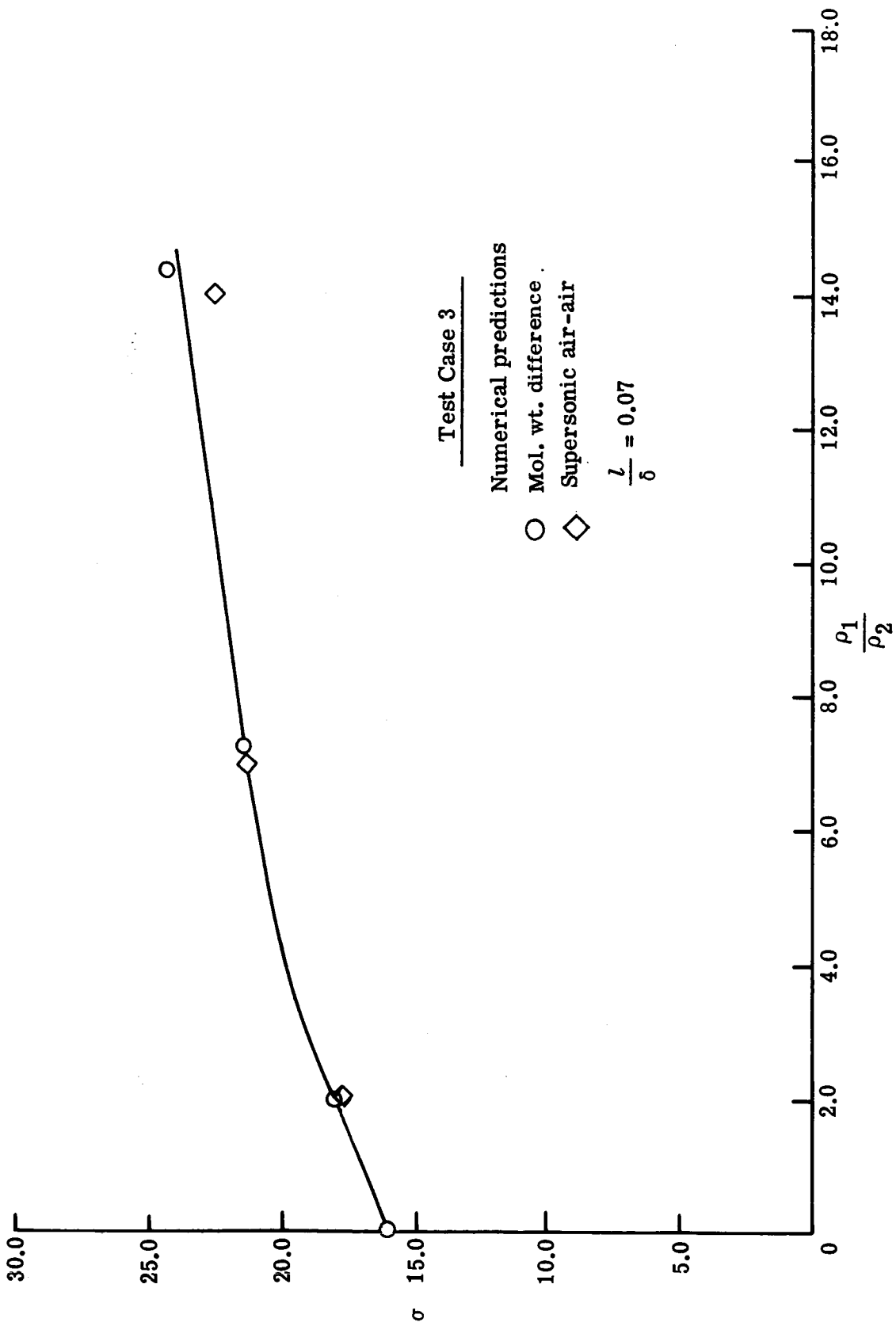
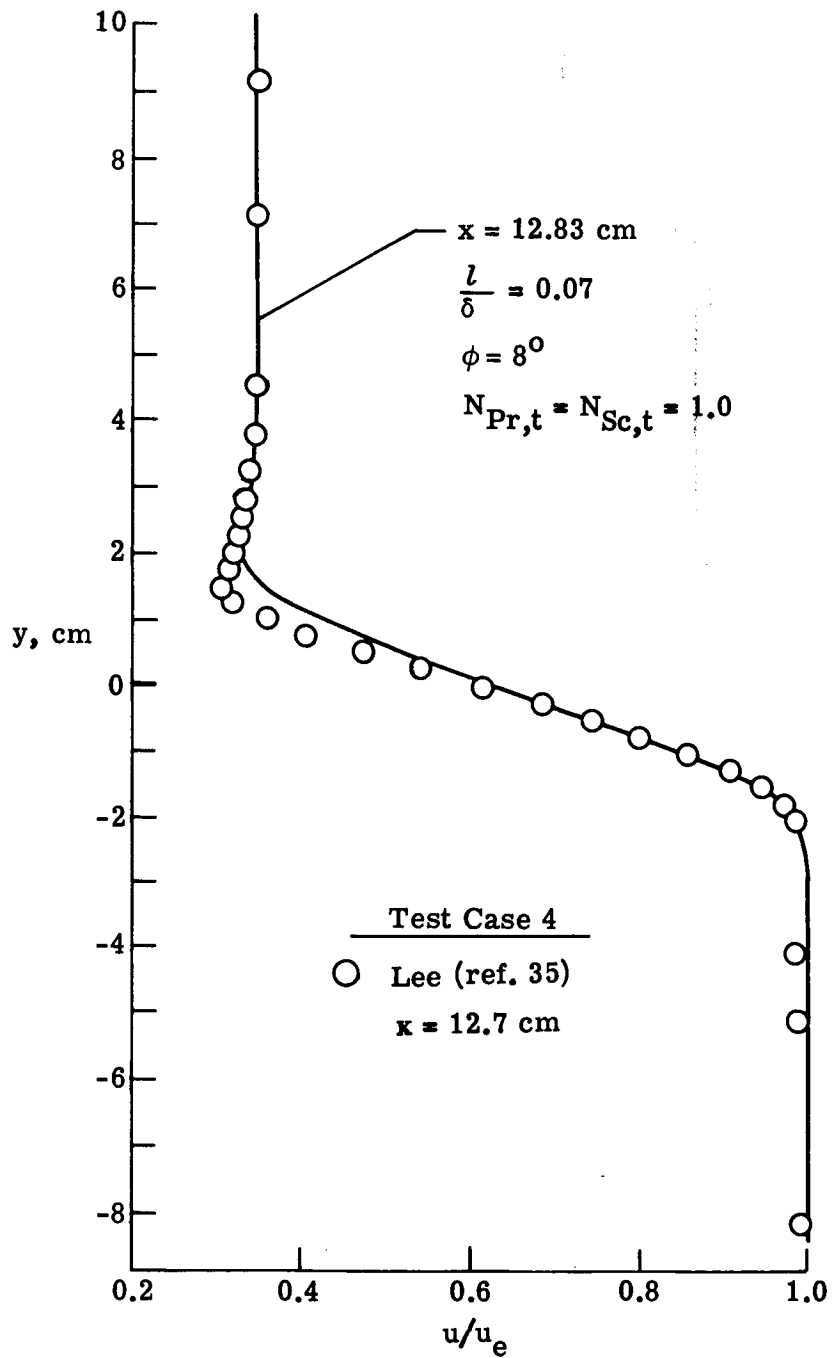
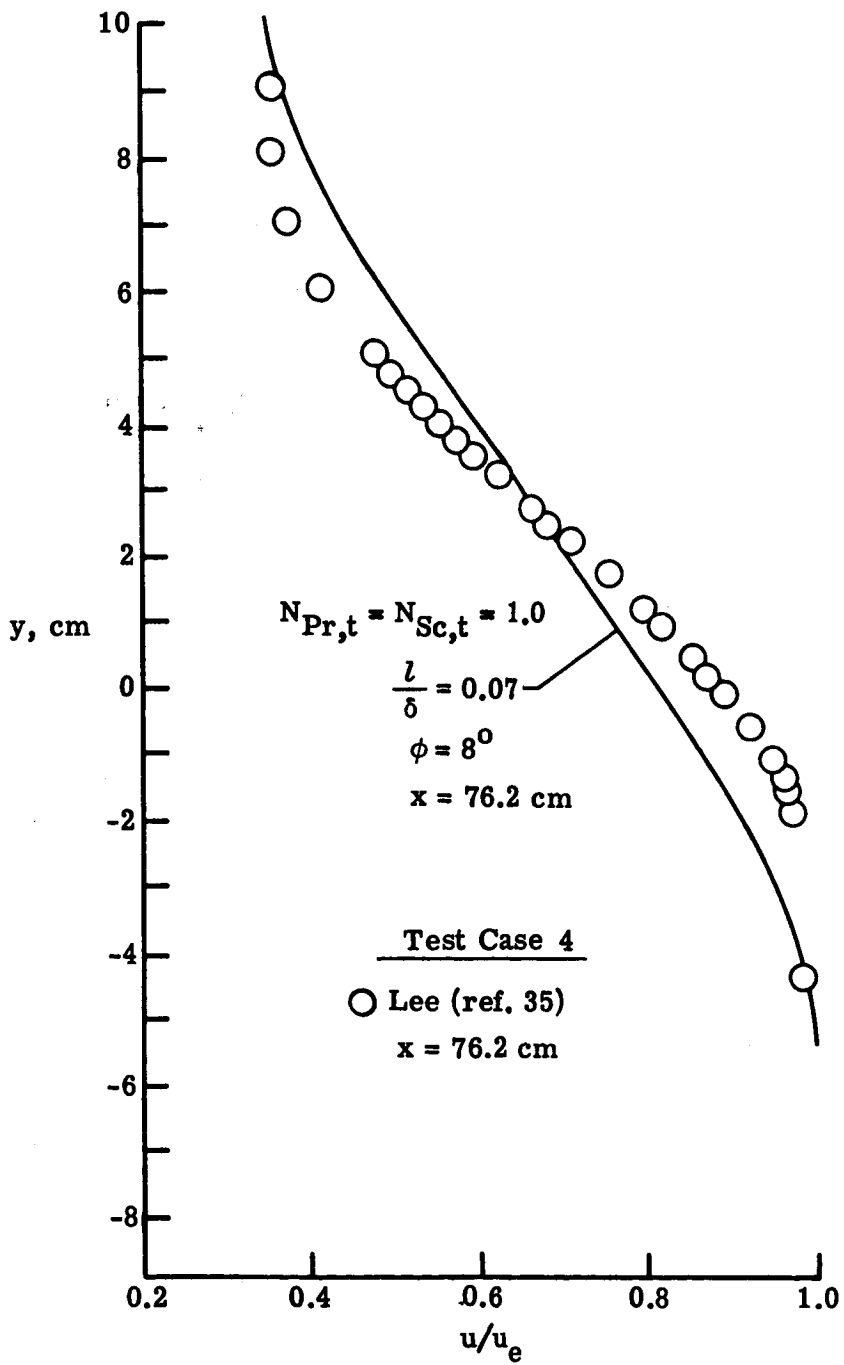


Figure 7.- Prediction of spreading parameter for two-dimensional variable-density free shear layers. Test case 3.



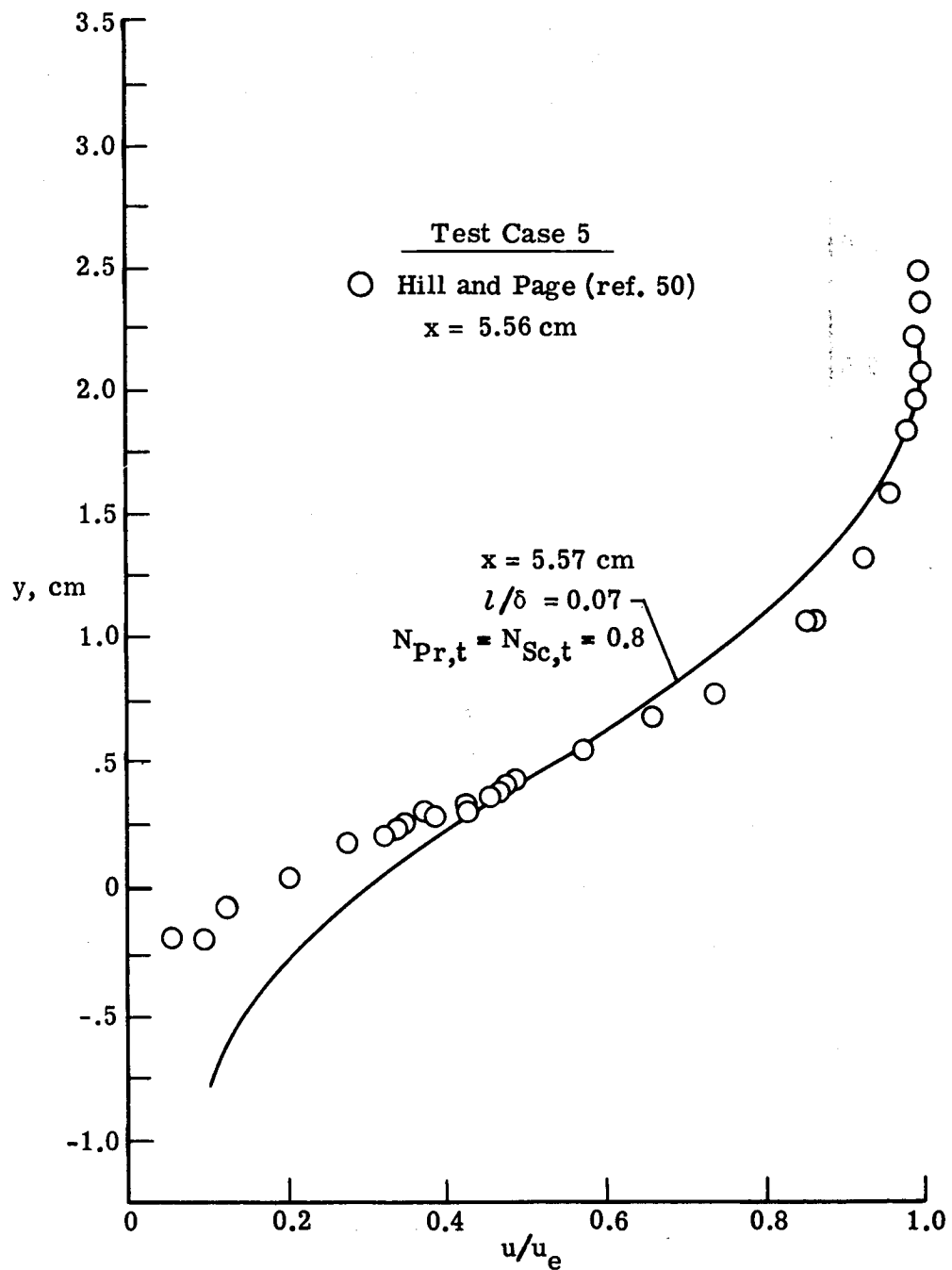
(a) $x = 12.7 \text{ cm}$.

Figure 8.- Predicted and experimental velocity profiles. Test case 4.



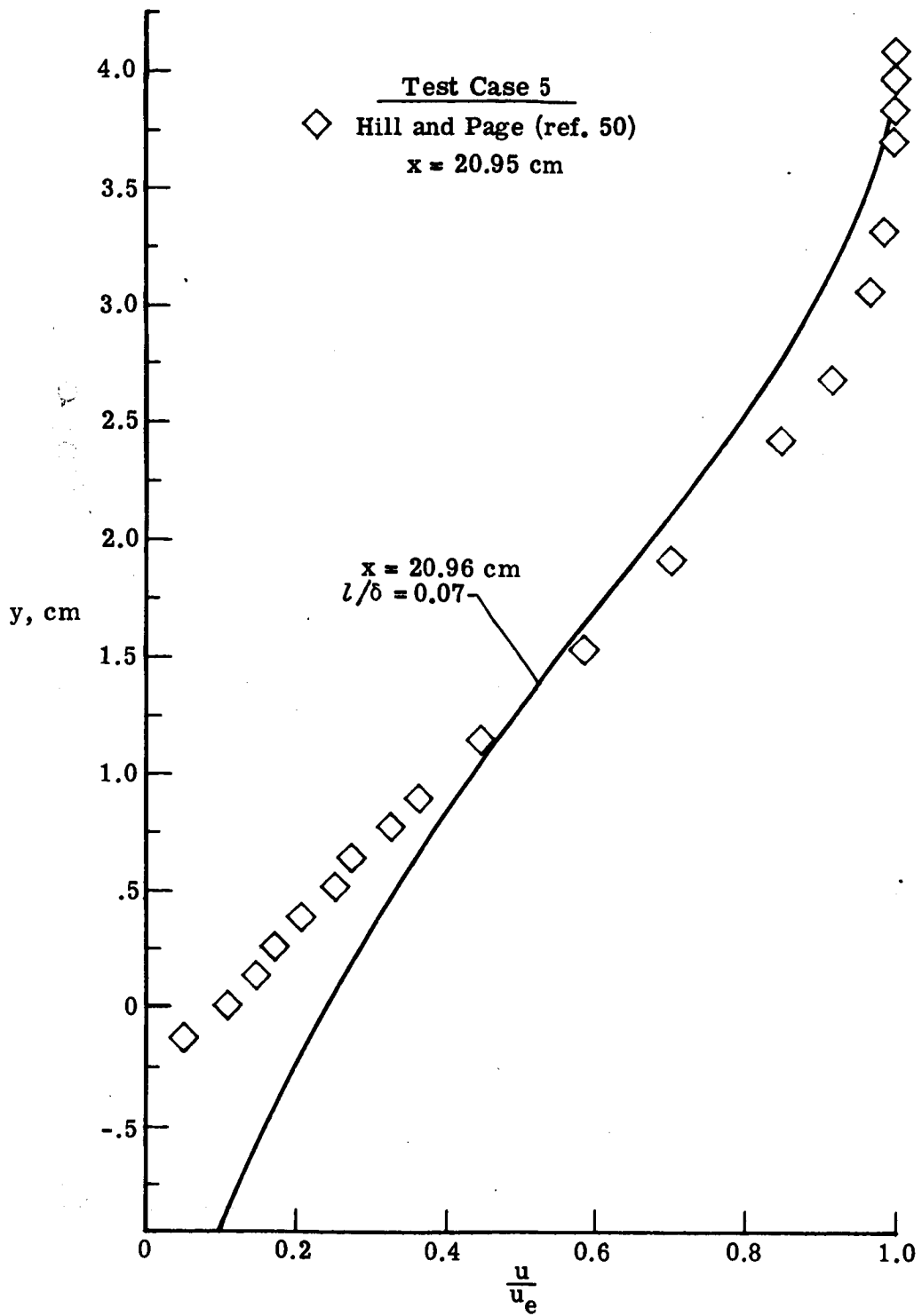
(b) $x = 76.2 \text{ cm}$.

Figure 8.- Concluded.



(a) x = 5.57 cm.

Figure 9.- Predicted and experimental velocity profiles. Test case 5.



(b) $x = 20.95 \text{ cm}$.

Figure 9.- Concluded.

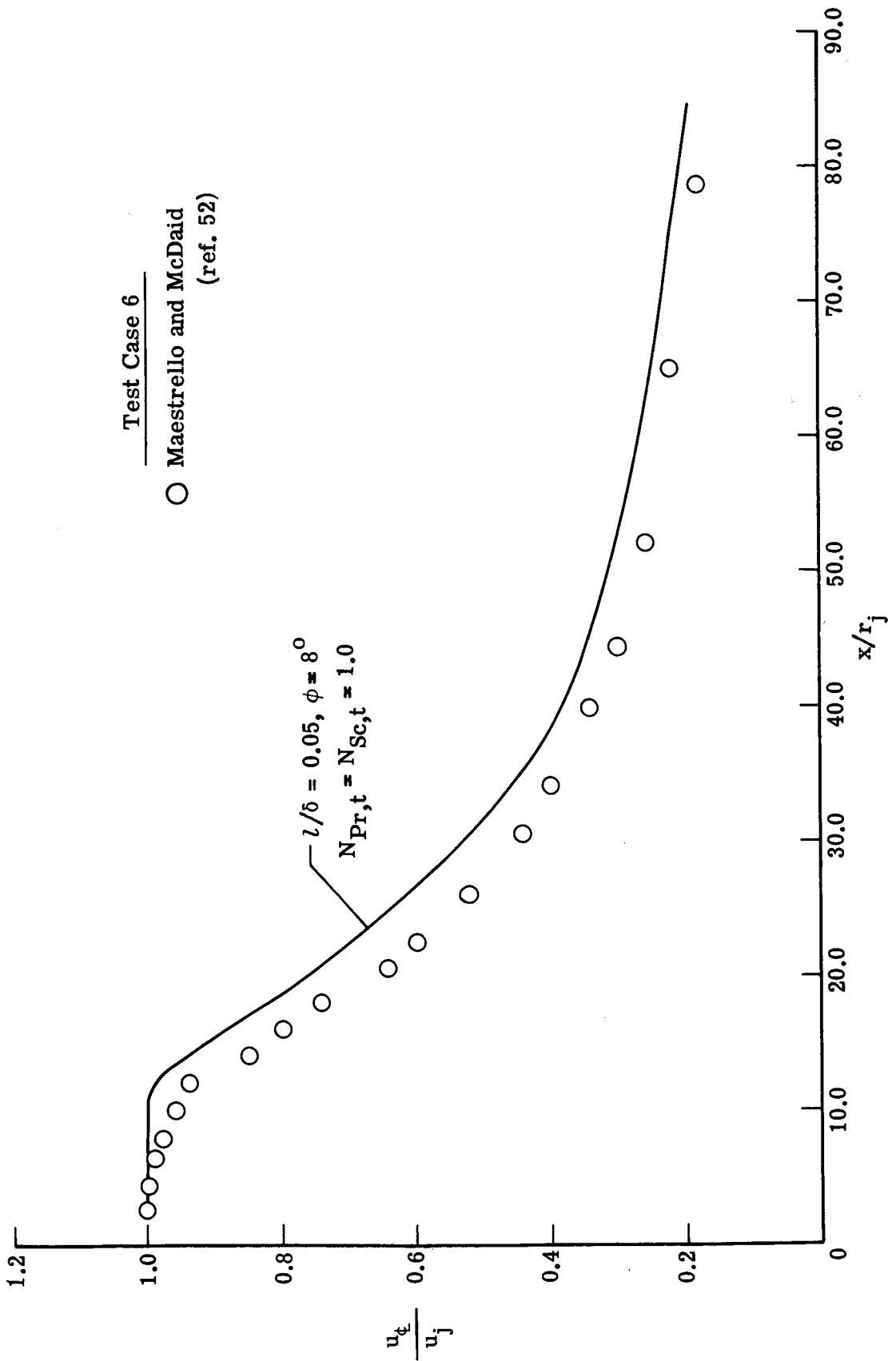
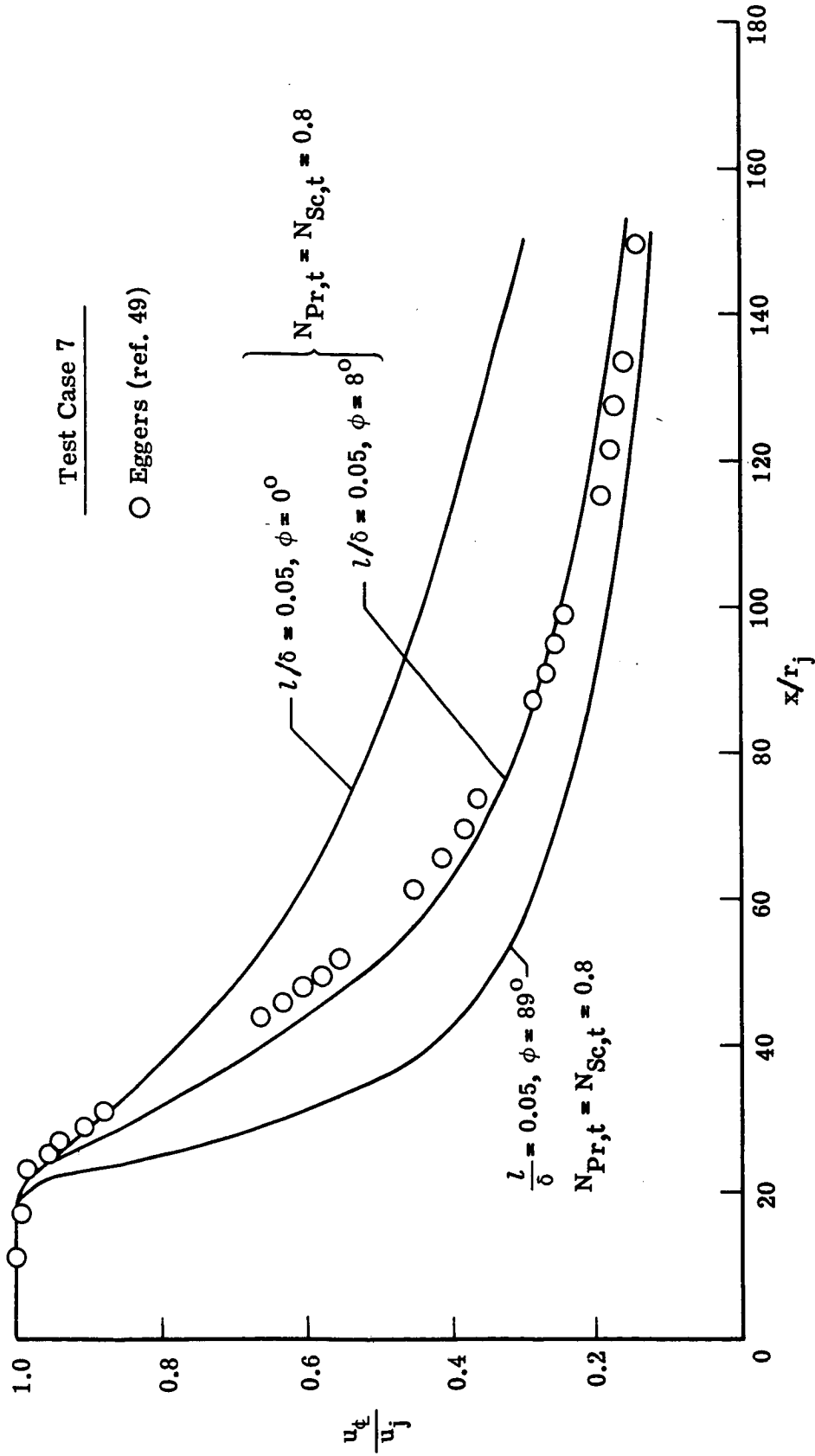


Figure 10.- Predicted and experimental center-line velocity distribution for a subsonic axisymmetric jet issuing into still air. Test case 6.



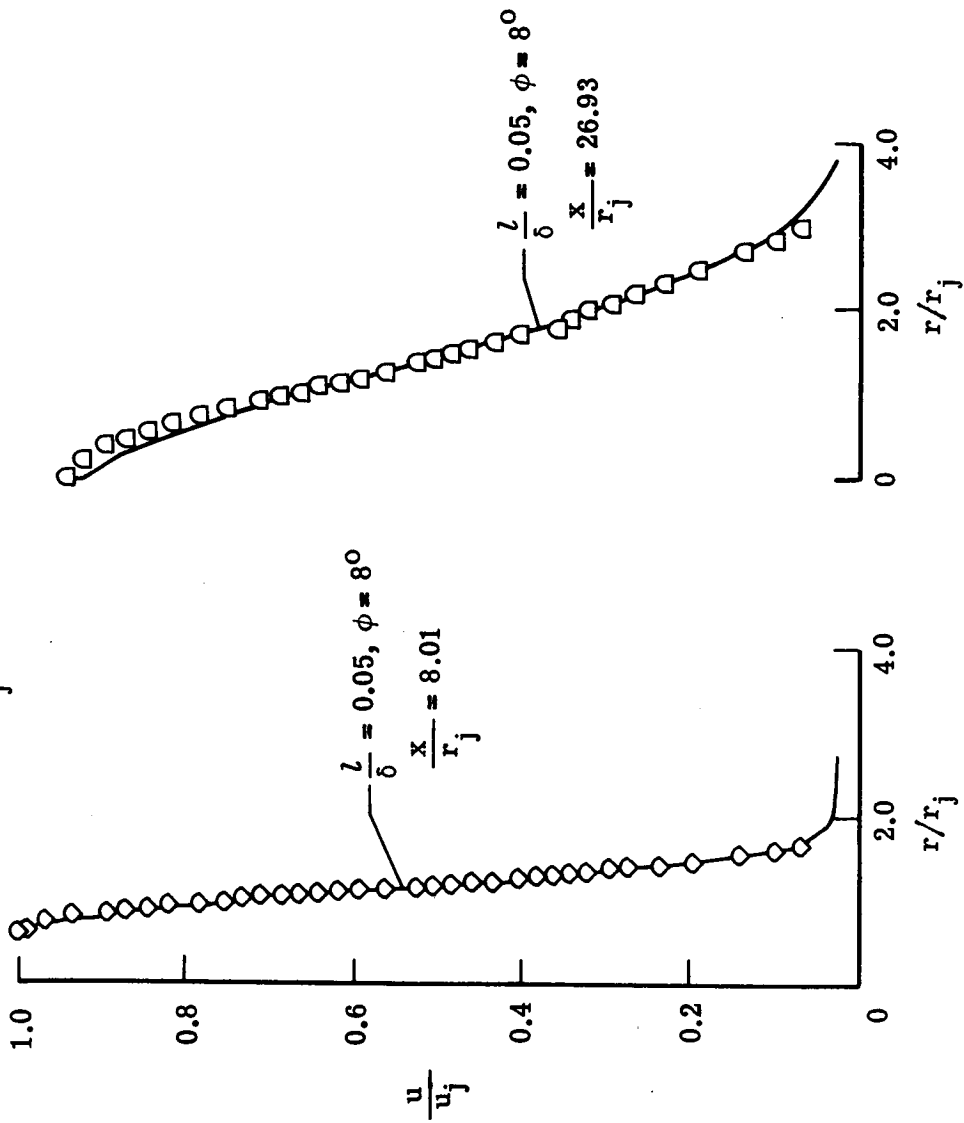
(a) Center-line distribution.

Figure 11.- Predicted and experimental velocity for a supersonic axisymmetric jet issuing into still air. Test case 7.

Test Case 7

\diamond $x/r_j = 8.02$
 \square $x/r_j = 26.93$

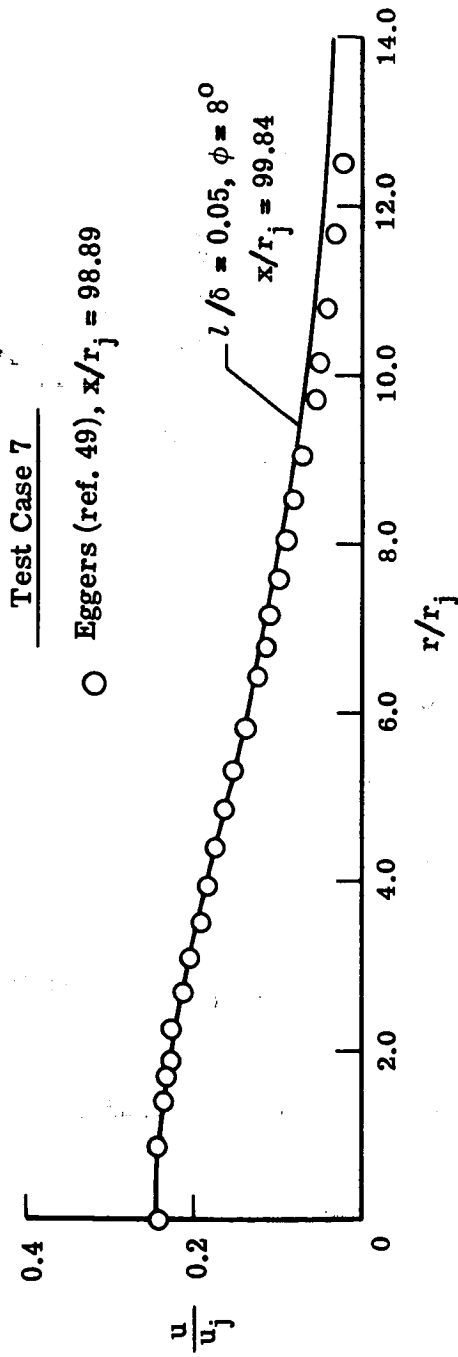
Eggers (ref. 49)



(b) Profiles at $x/r_j \approx 8$.

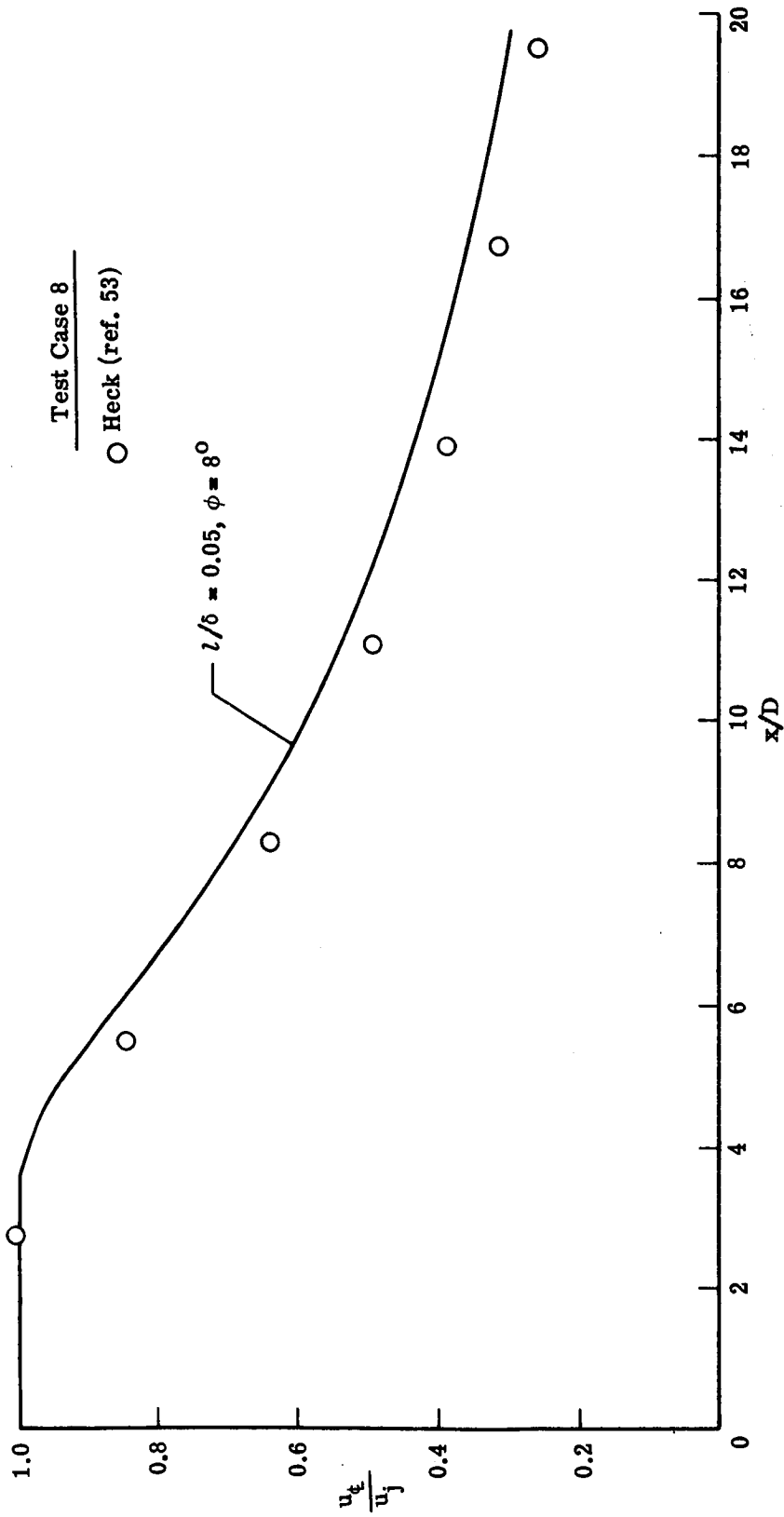
(c) Profiles at $x/r_j \approx 27$.

Figure 11.- Continued.



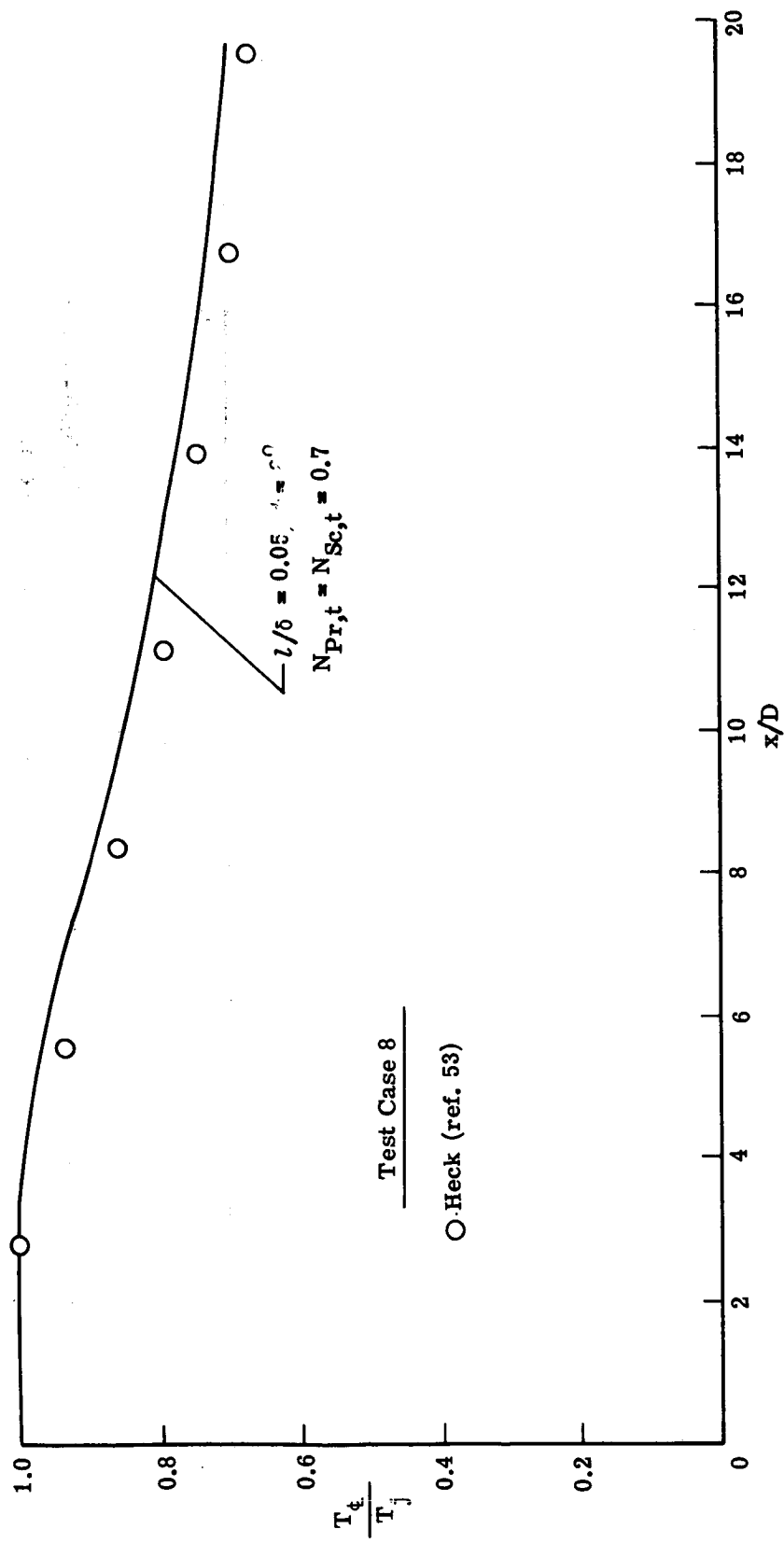
(d) Profiles at $x/r_j \approx 99$.

Figure 11.- Concluded.



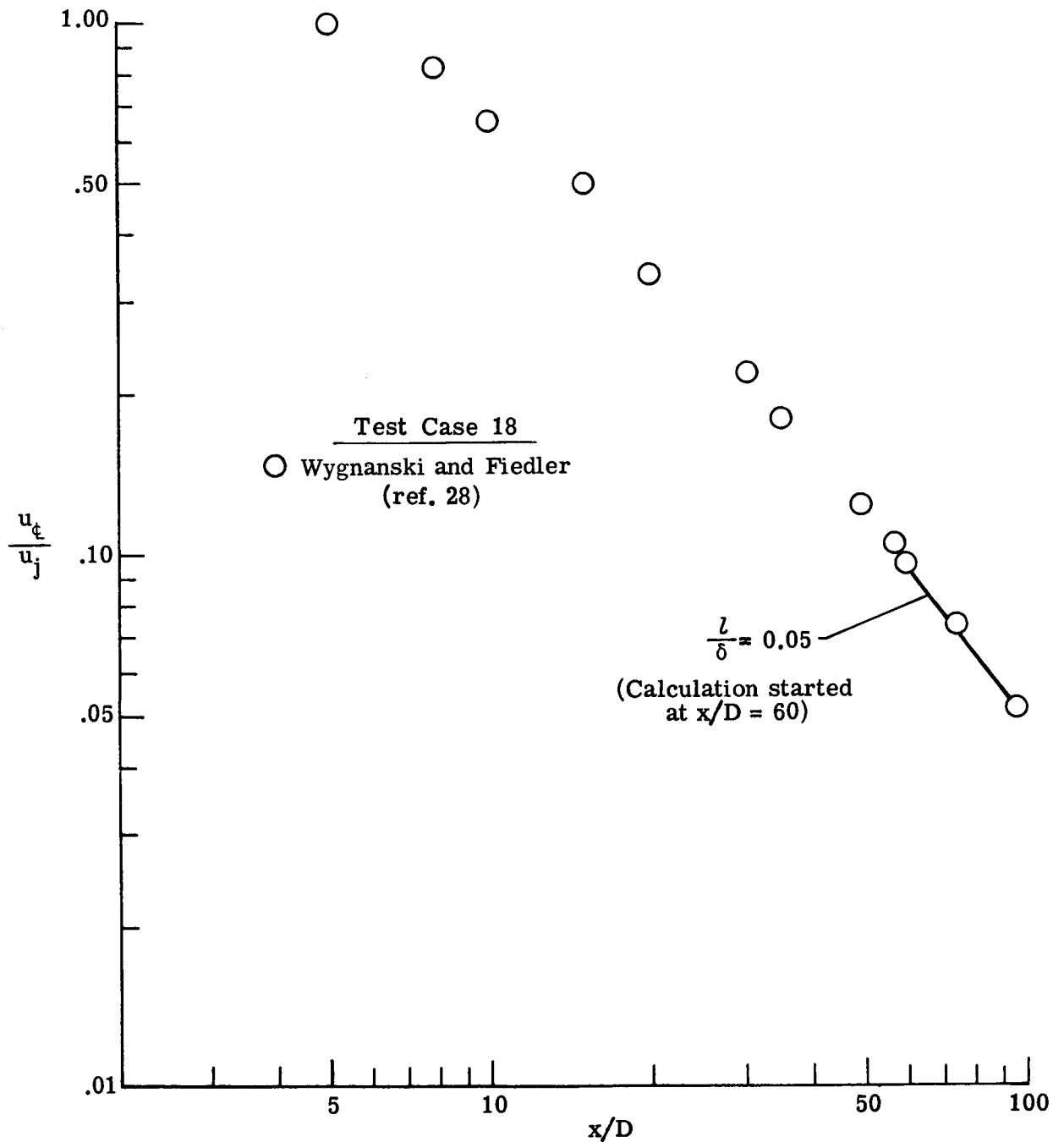
(a) Velocity.

Figure 12.- Predicted and experimental center-line distribution for high-temperature axisymmetric jet issuing into still air. Test case 8.



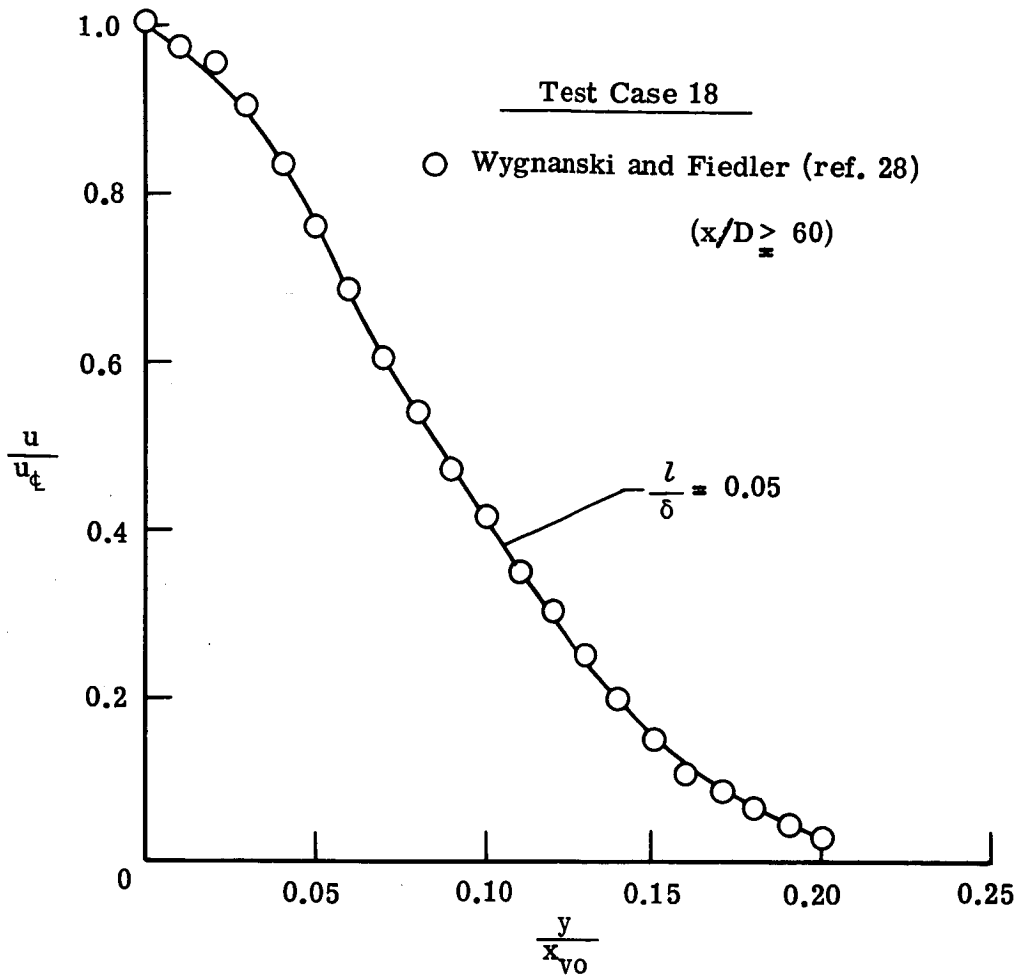
(b) Static temperature.

Figure 12.- Concluded.



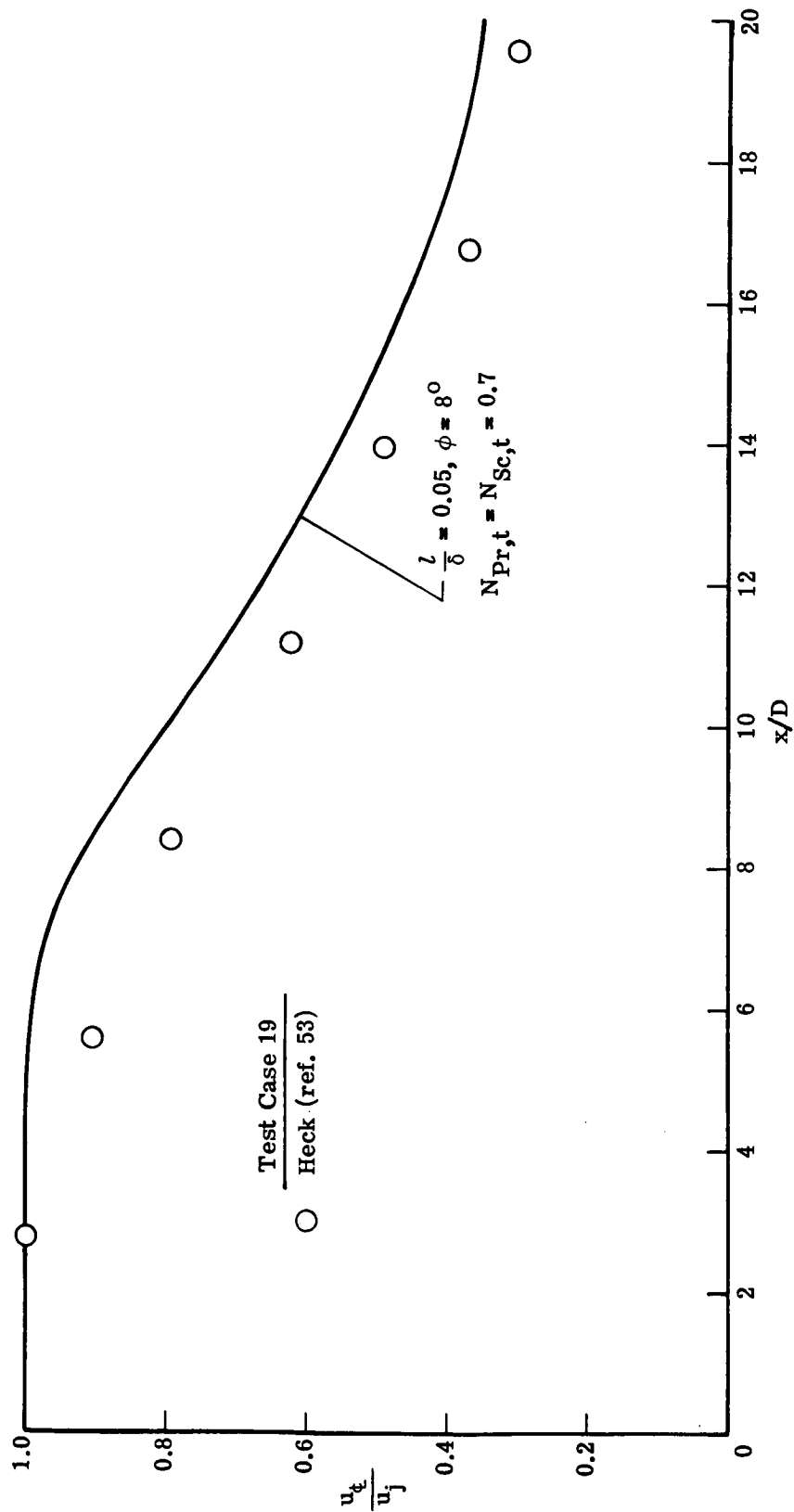
(a) Center-line distribution.

Figure 13.- Predicted and experimental velocity for the far field of an axisymmetric jet issuing into still air. Test case 18.



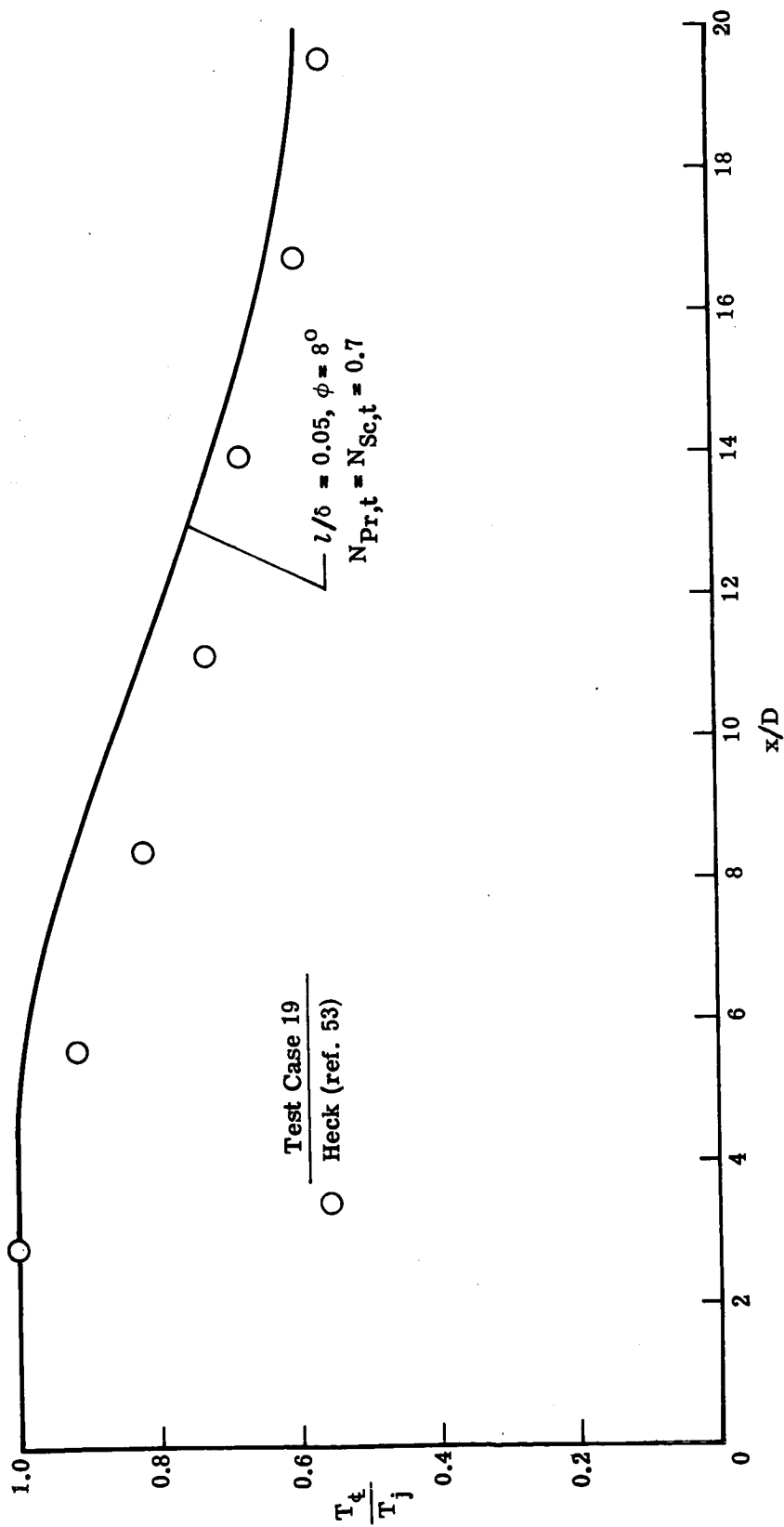
(b) Similarity profiles.

Figure 13.- Concluded.



(a) Velocity.

Figure 14.- Predicted and experimental center-line distribution for high-temperature supersonic axisymmetric jet issuing into still air. Test case 19.



(b) Static temperature.

Figure 14.- Concluded.

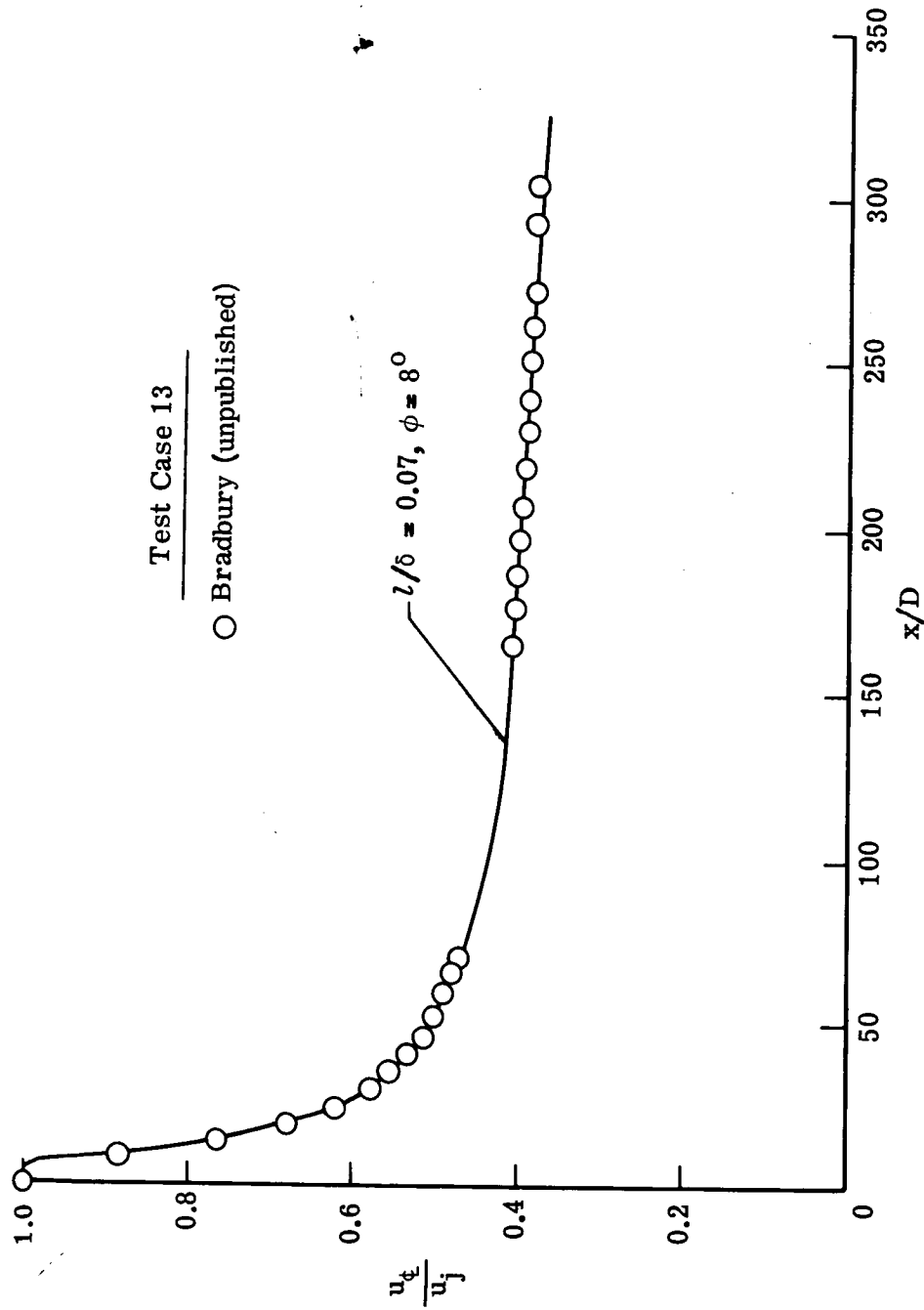


Figure 15.- Predicted and experimental center-line velocity for two-dimensional jet in a moving stream. Test case 13.

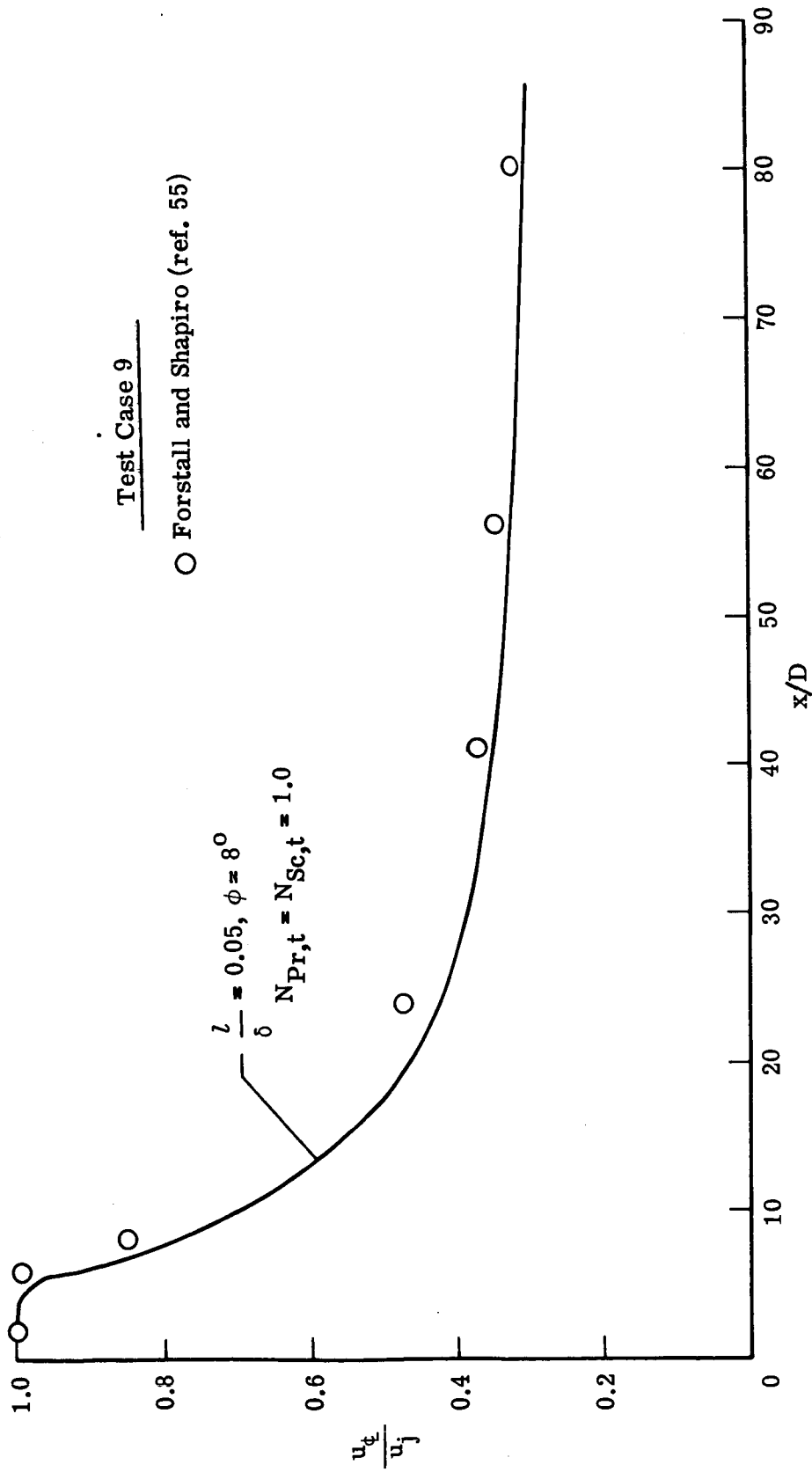
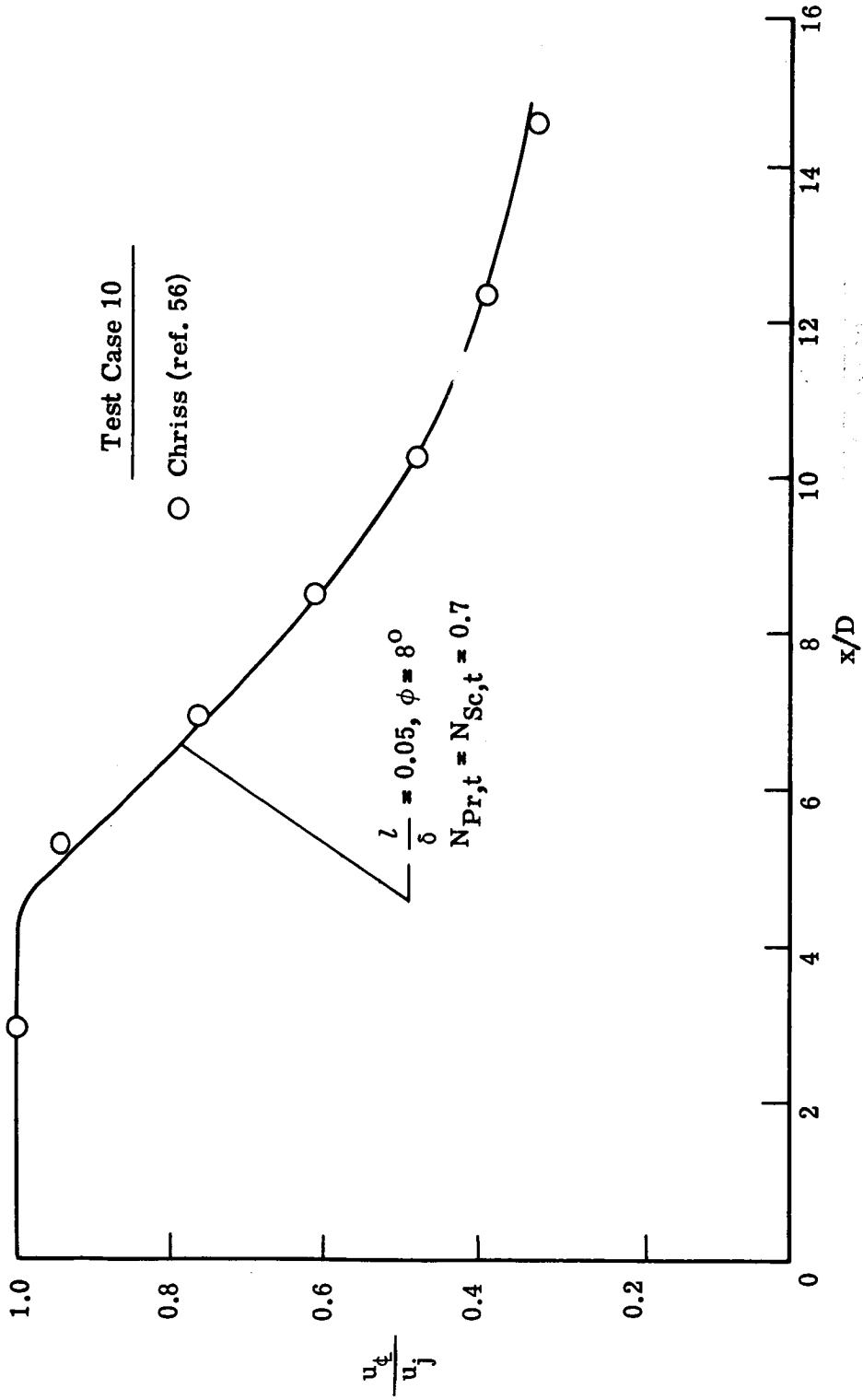
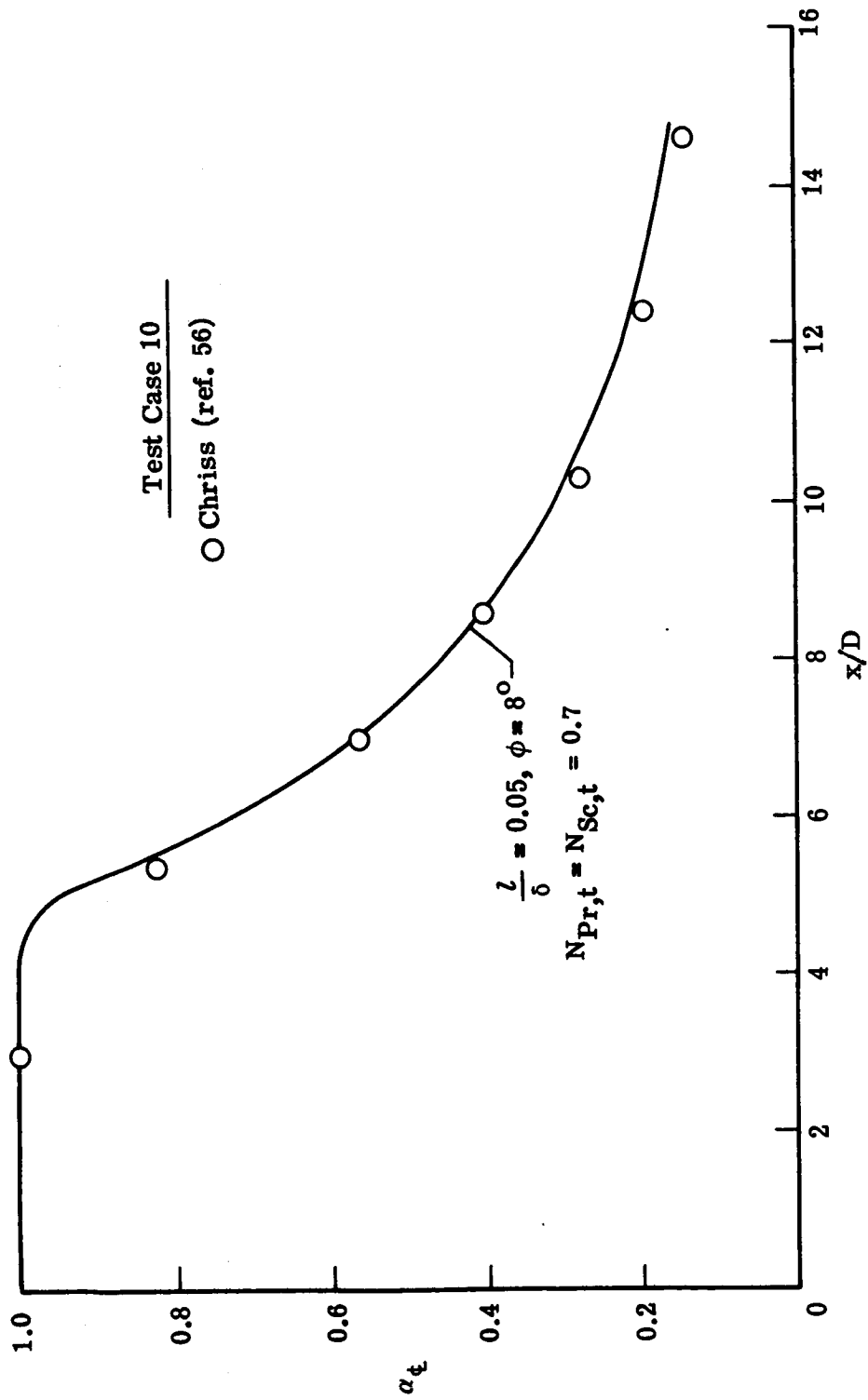


Figure 16.- Predicted and experimental center-line velocity for coaxial air jets. Test case 9.



(a) Velocity.

Figure 17.- Predicted and experimental center-line distribution for subsonic hydrogen-air coaxial flow. Test case 10.



(b) Mass fraction of hydrogen.

Figure 17.- Concluded.

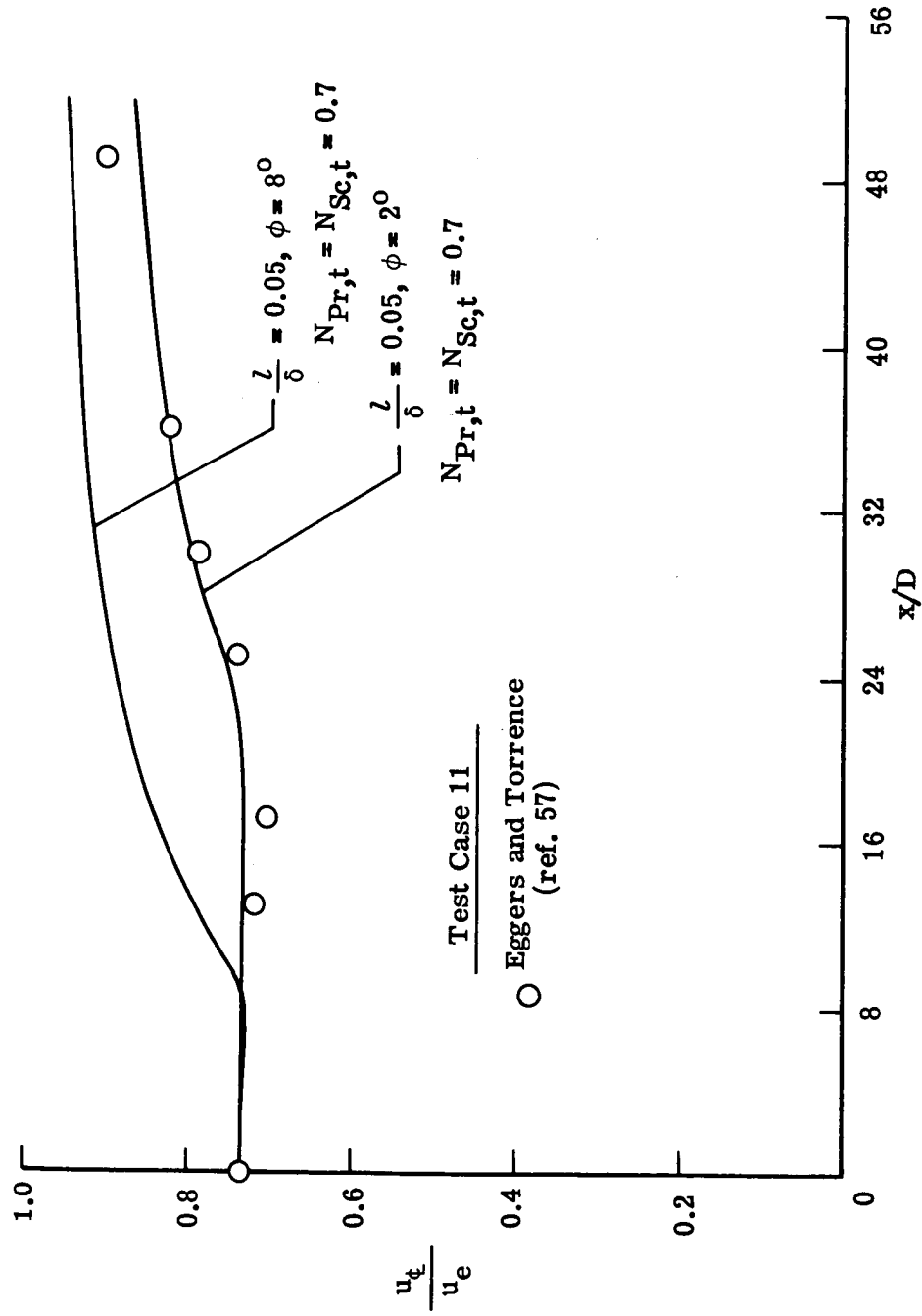
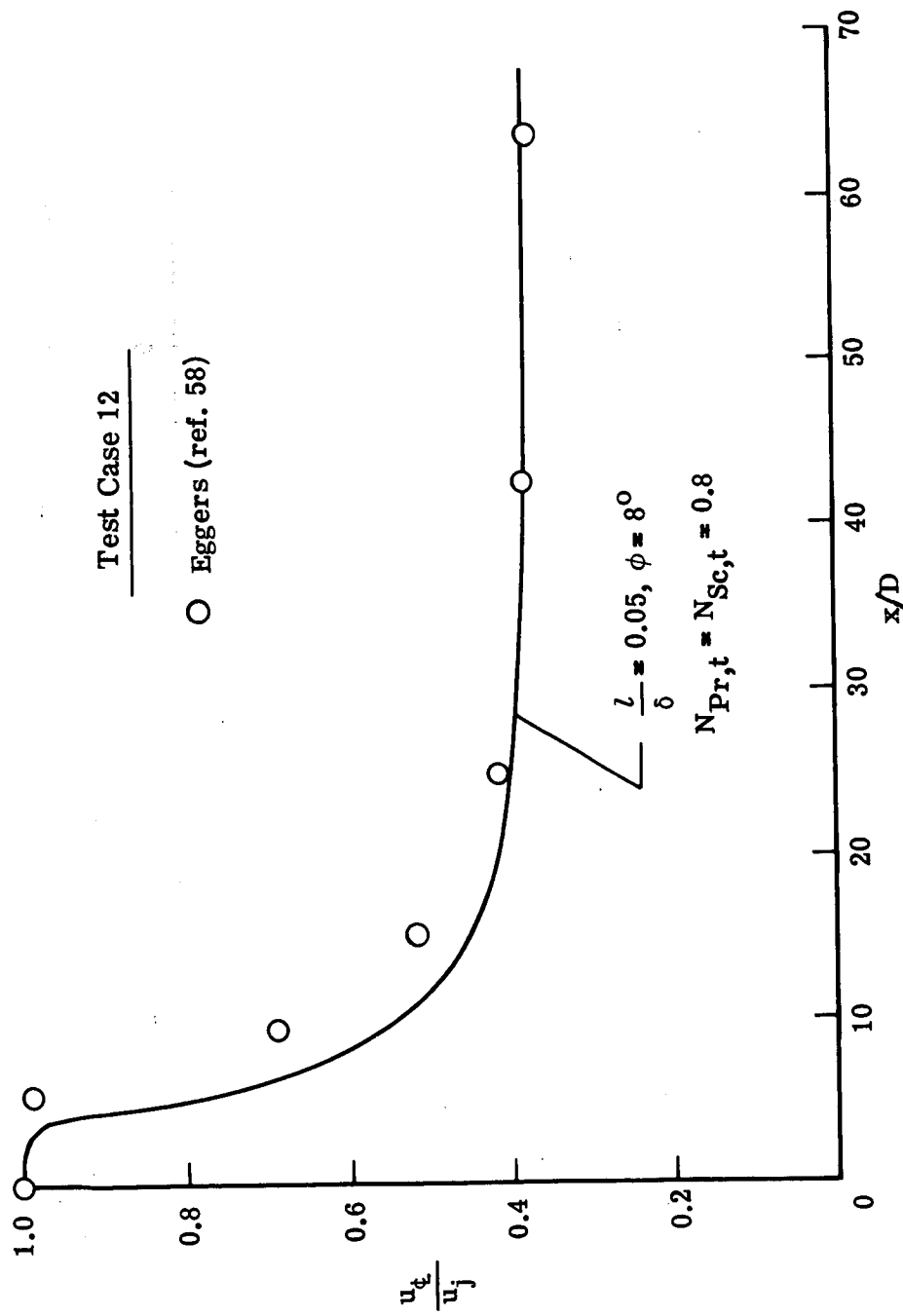
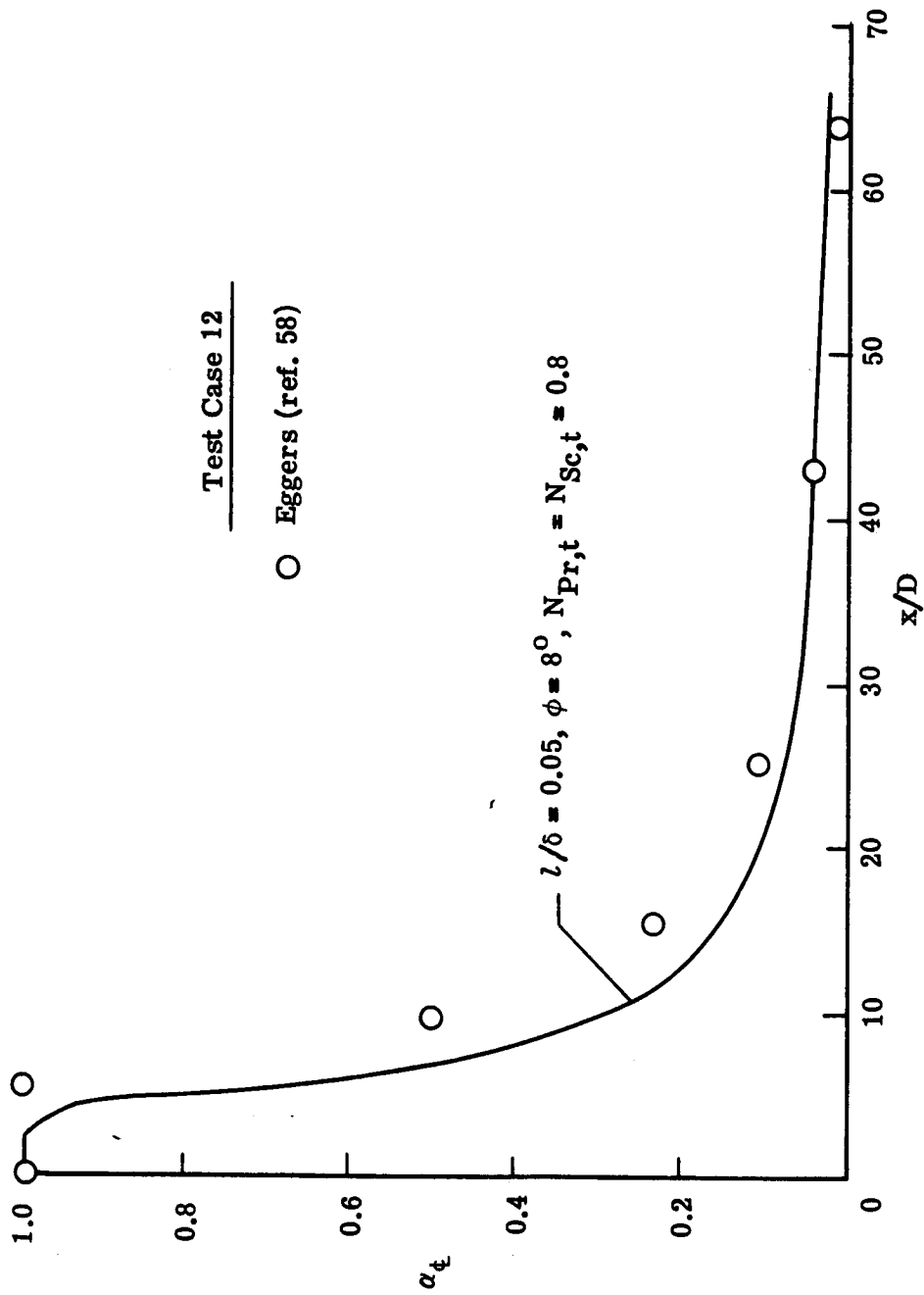


Figure 18.- Predicted and experimental center-line velocity for air-air coaxial jets. Test case 11.



(a) Velocity.

Figure 19.- Predicted and experimental center-line distribution for hydrogen-air coaxial jets. Test case 12.



(b) Mass fraction of hydrogen.

Figure 19.- Concluded.

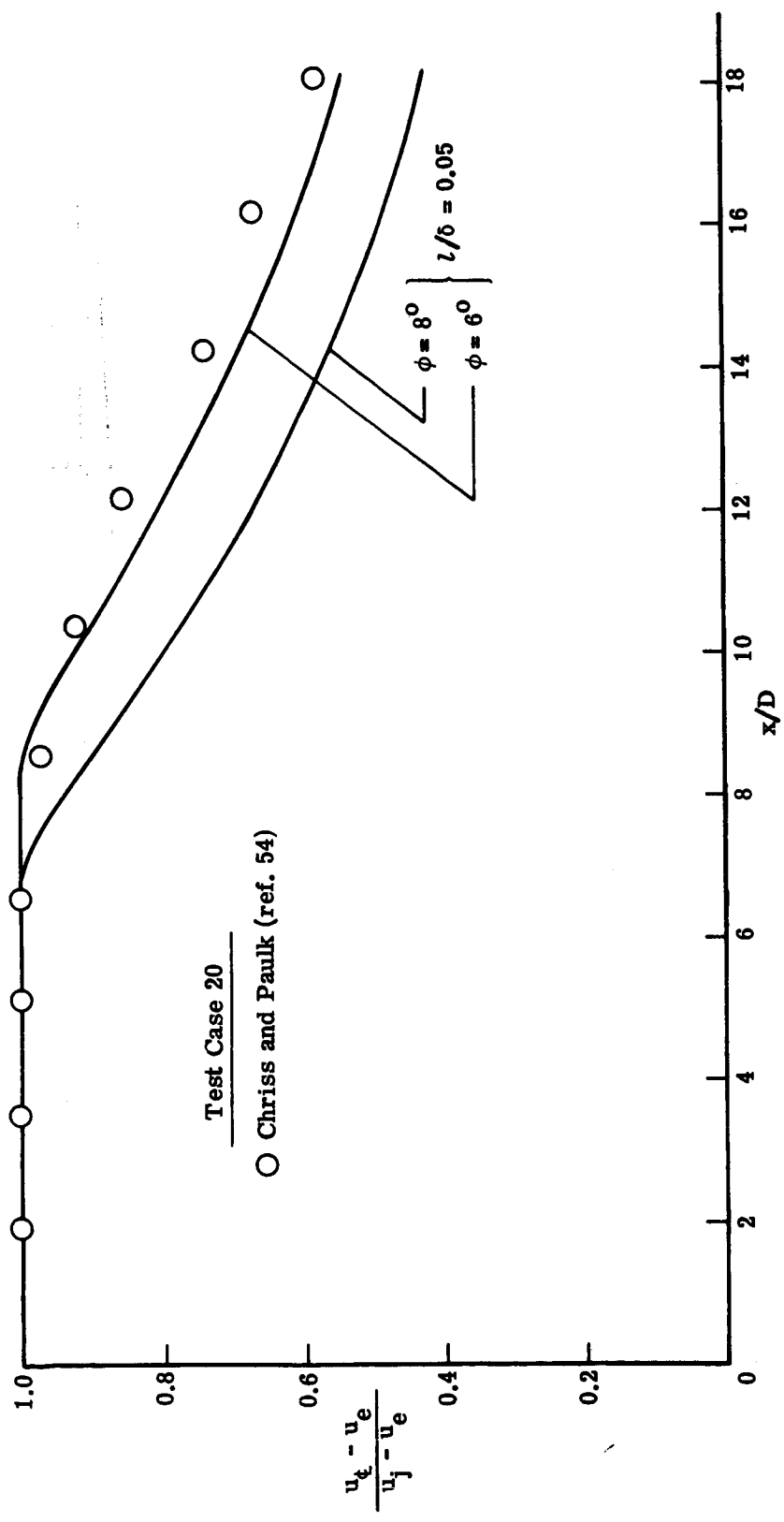
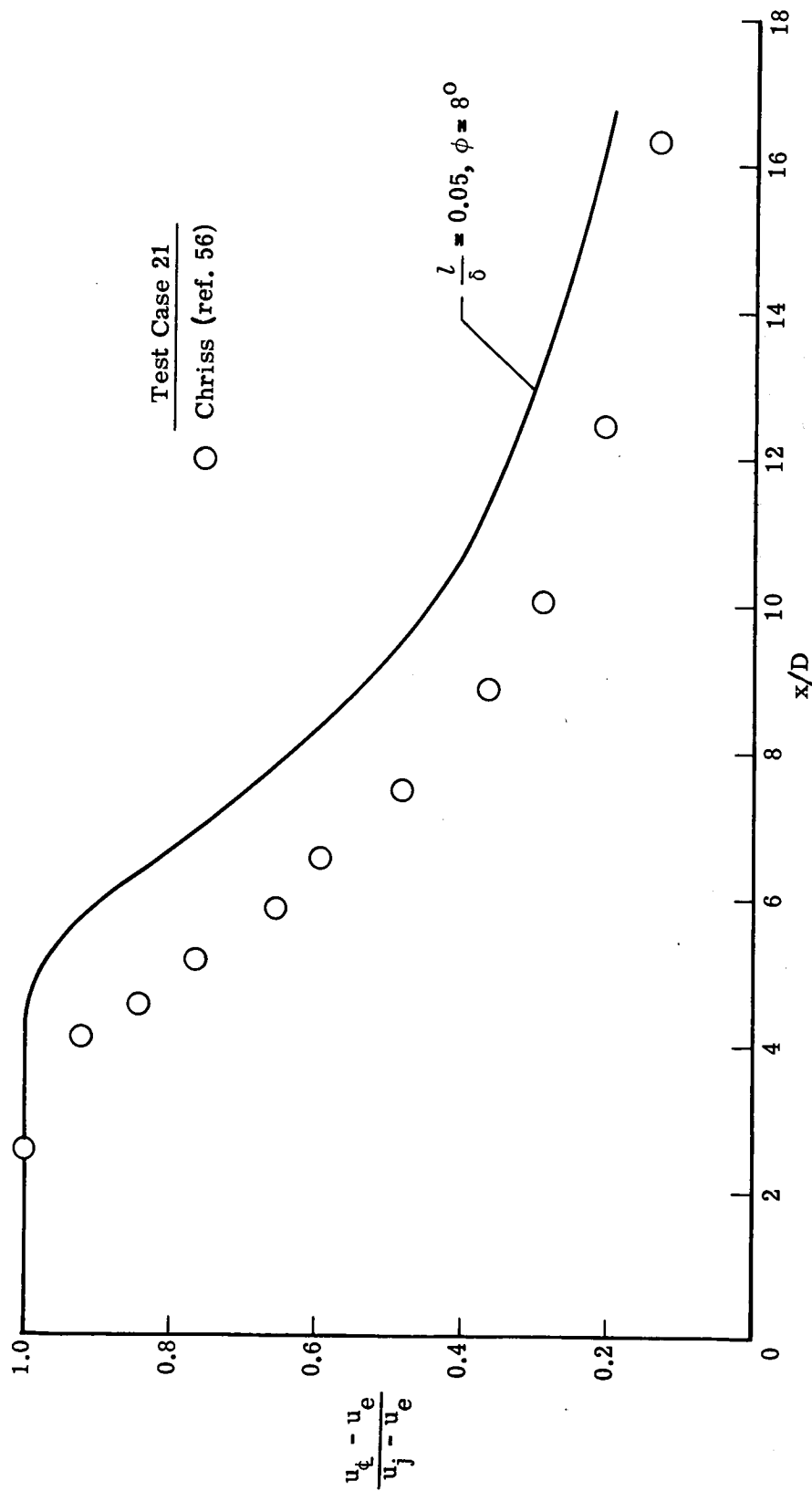
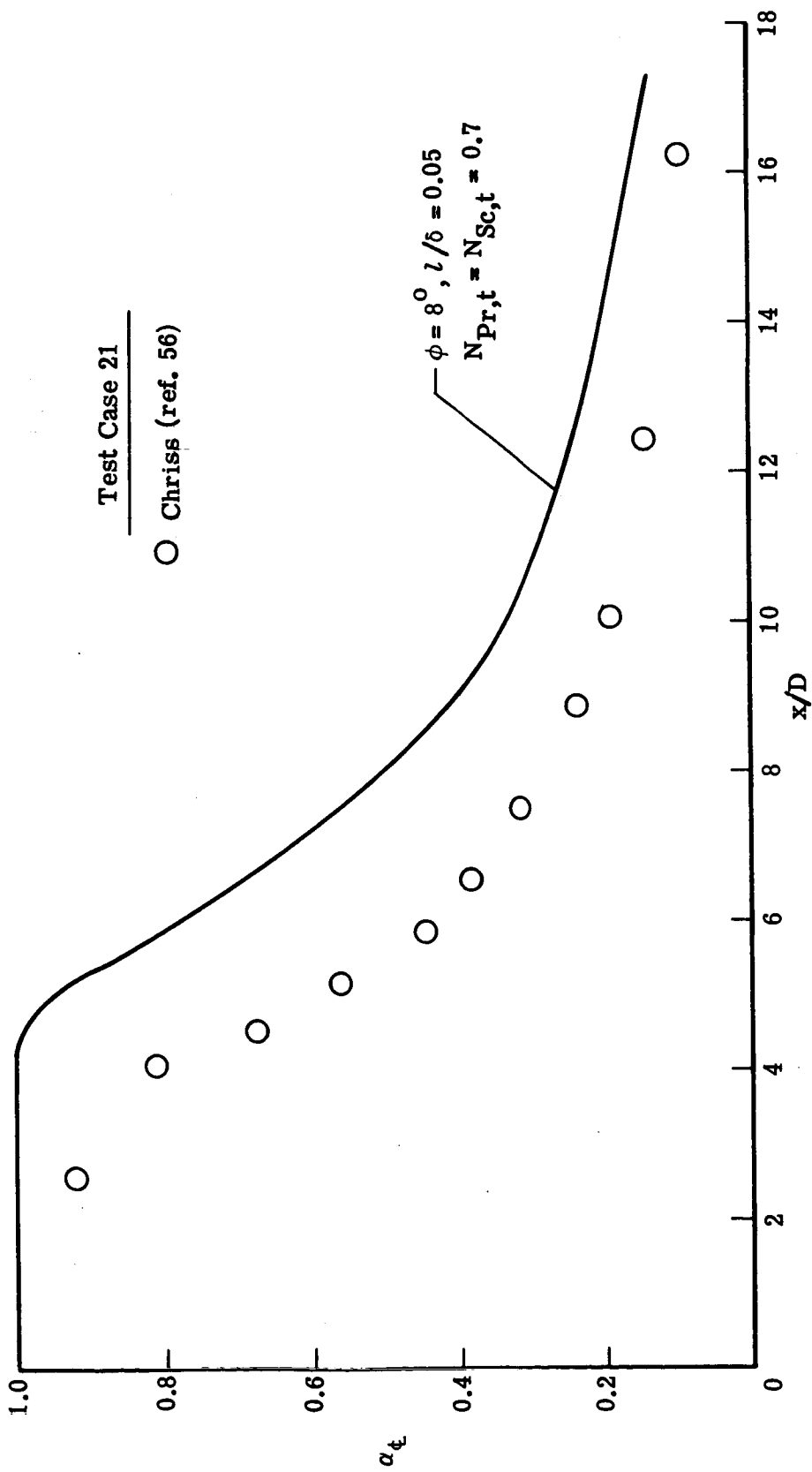


Figure 20.- Predicted and experimental center-line velocity for subsonic coaxial air jets. Test case 20.



(a) Velocity.

Figure 21.- Predicted and experimental center-line distribution for subsonic hydrogen-air coaxial mixing. Test case 21.



(b) Mass fraction of hydrogen.

Figure 21.- Concluded.

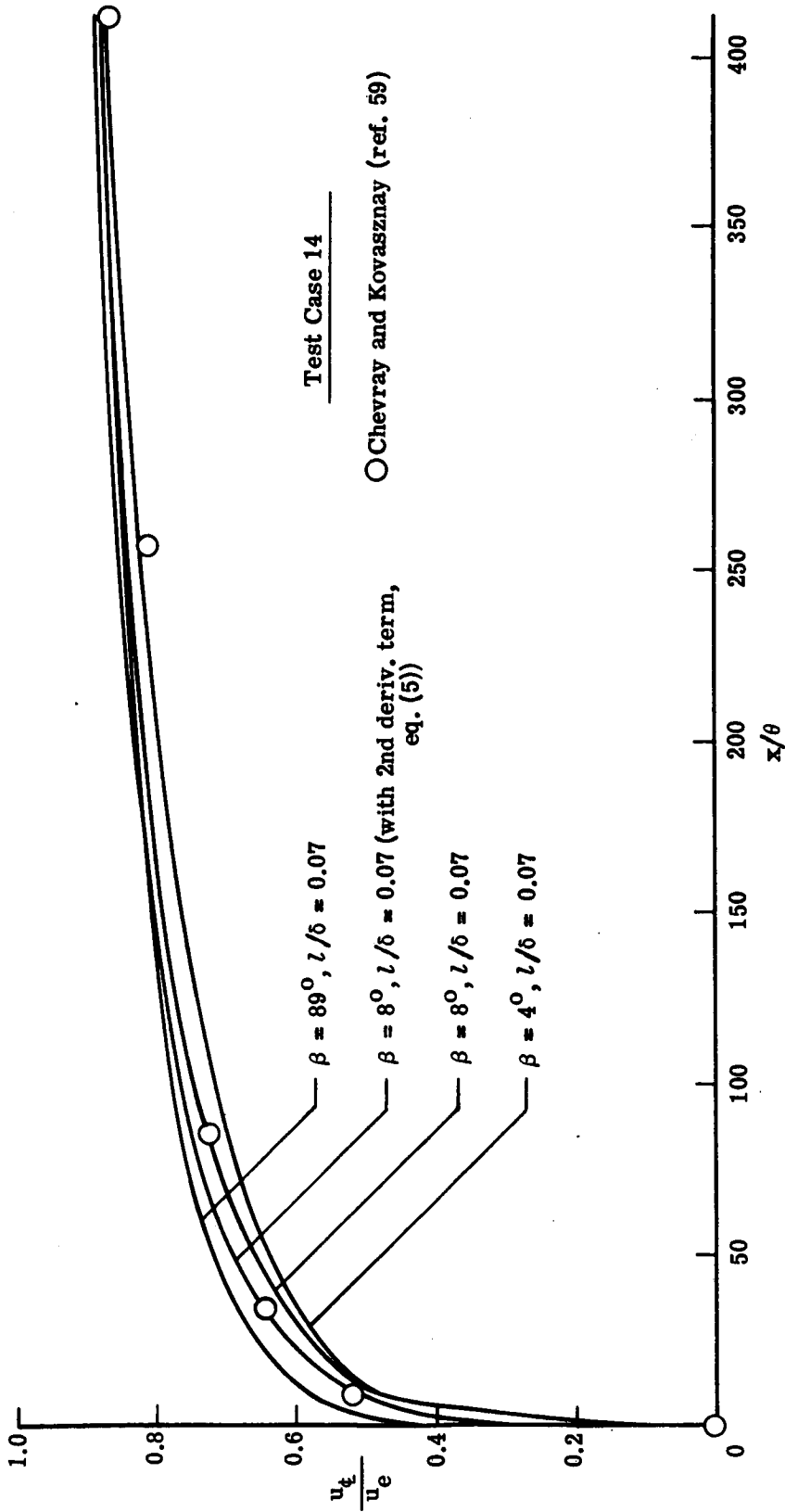


Figure 22.- Predicted and experimental center-line velocity for a two-dimensional subsonic wake. Test case 14.

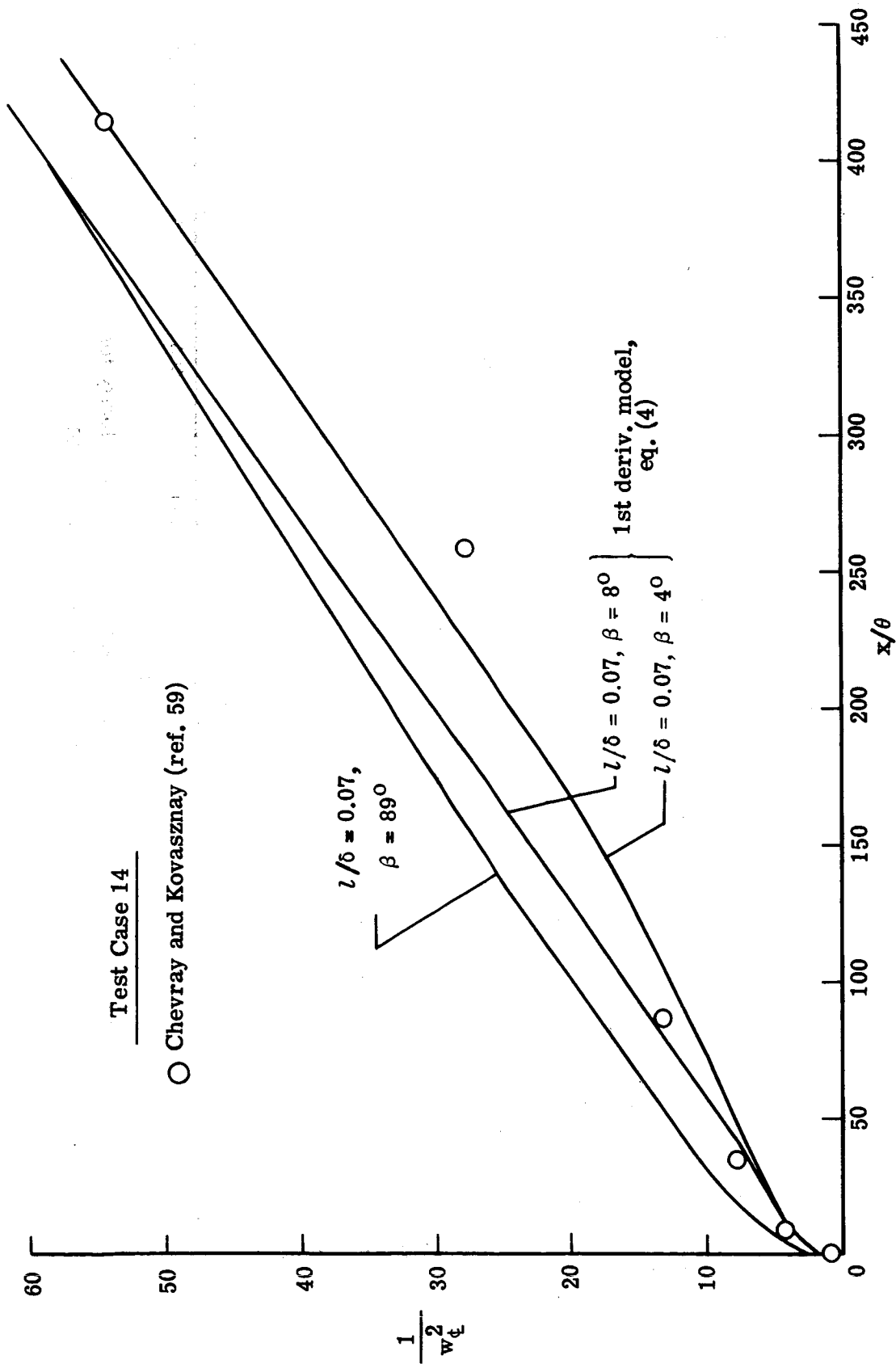


Figure 22.- Concluded.

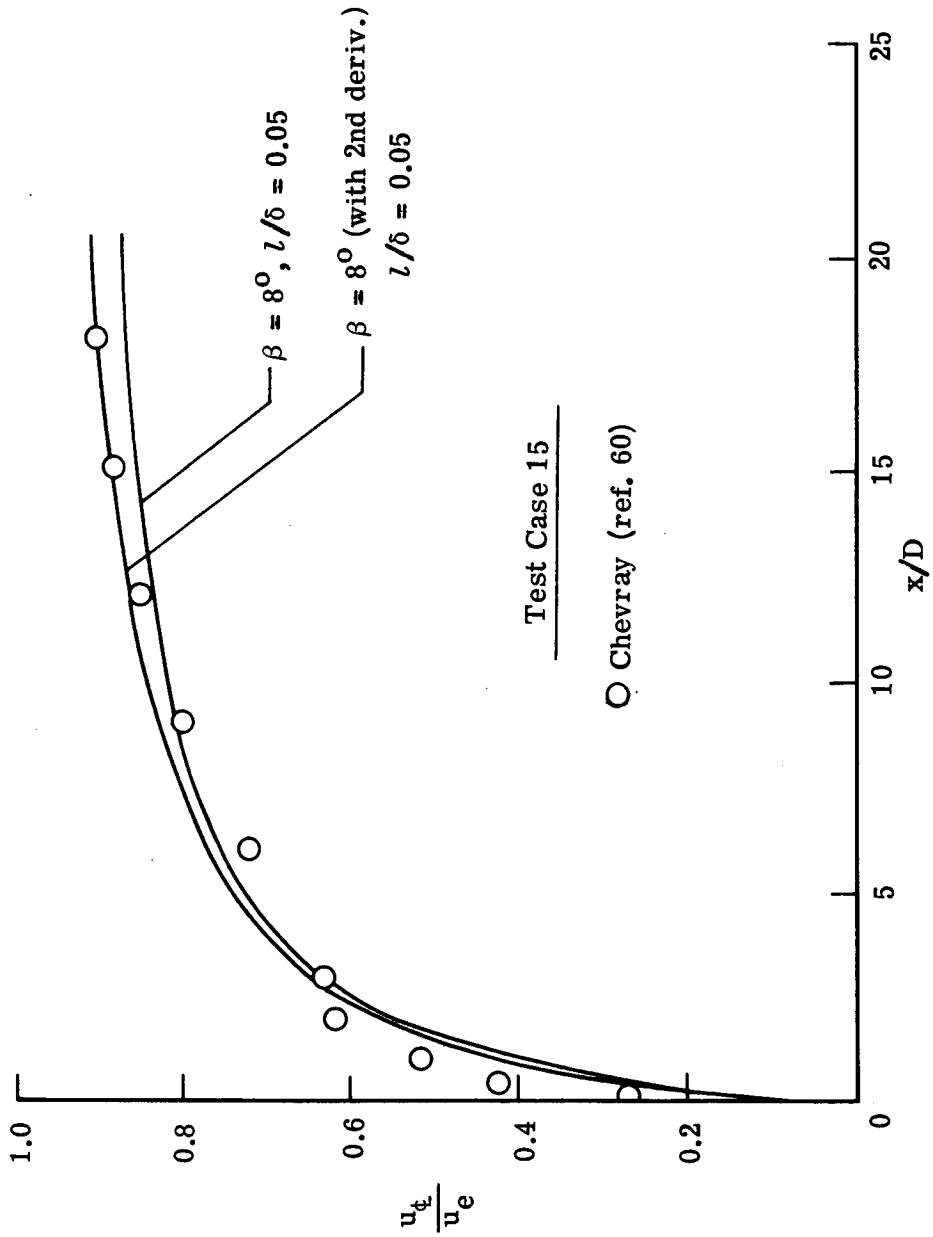
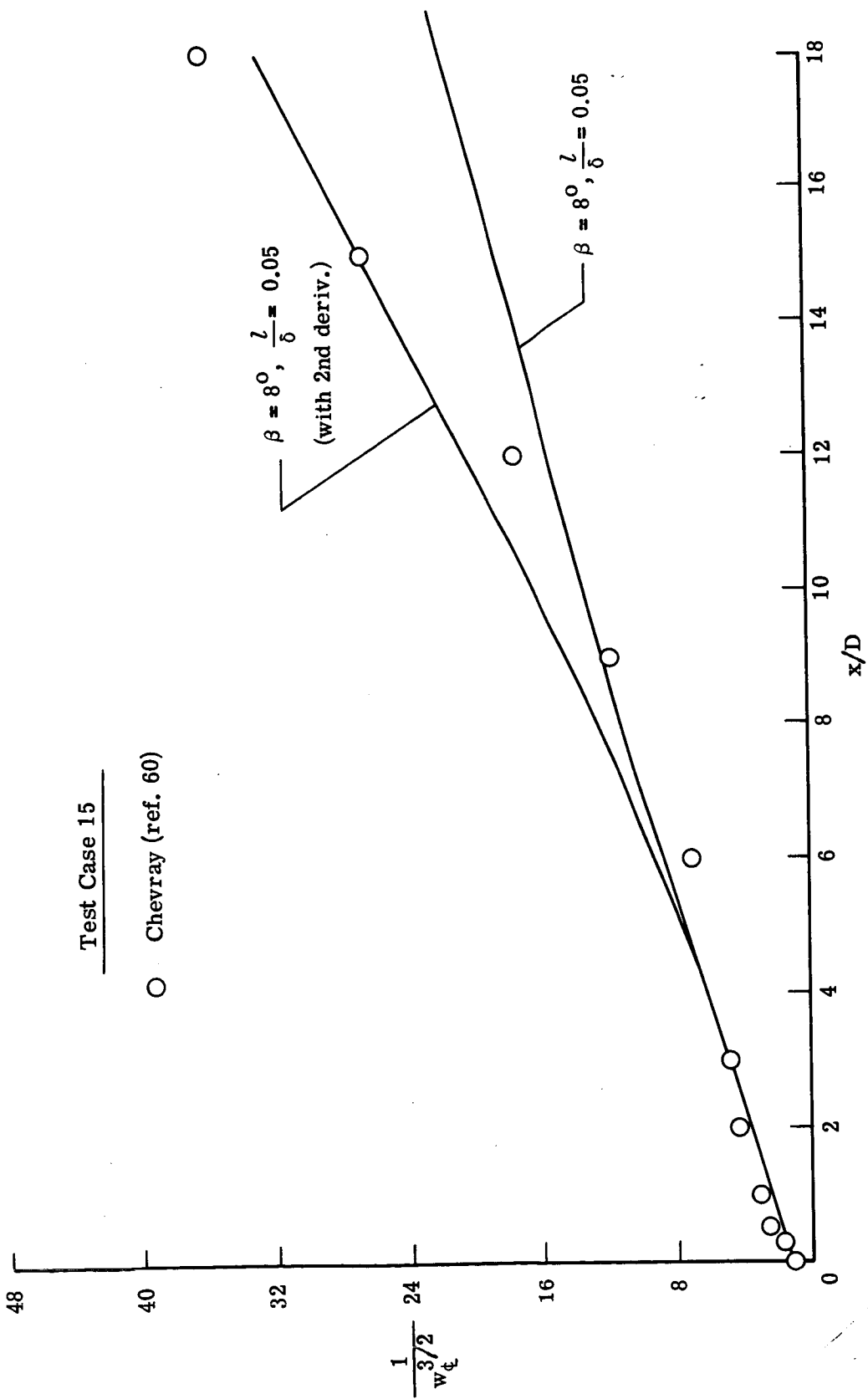


Figure 23.- Predicted and experimental center-line velocity for a subsonic axisymmetric wake. Test case 15.



Test Case 15

○ Chevray (ref. 60)

Figure 23.- Concluded.

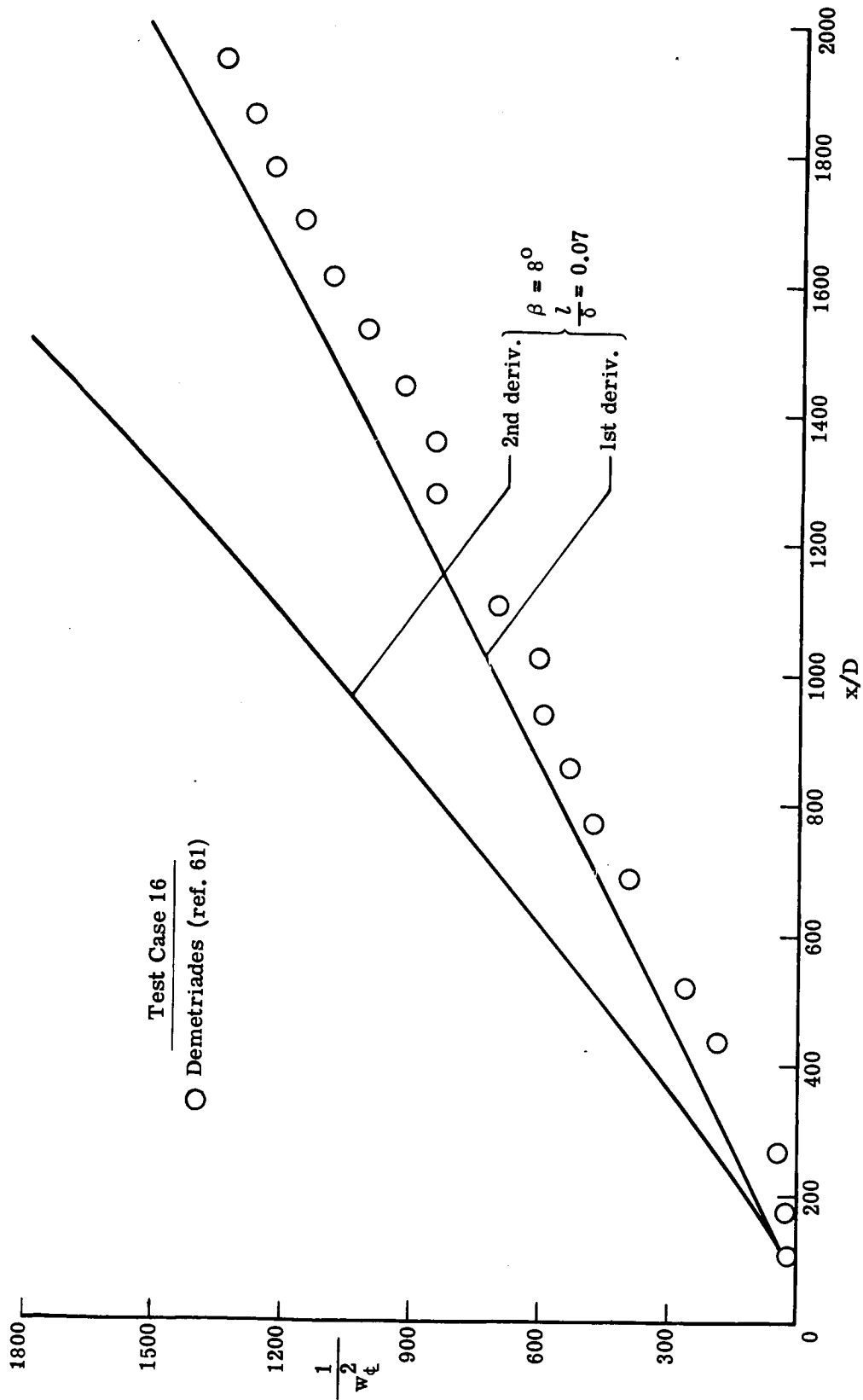


Figure 24.- Predicted and experimental center-line velocity for a two-dimensional supersonic wake. Test case 16.

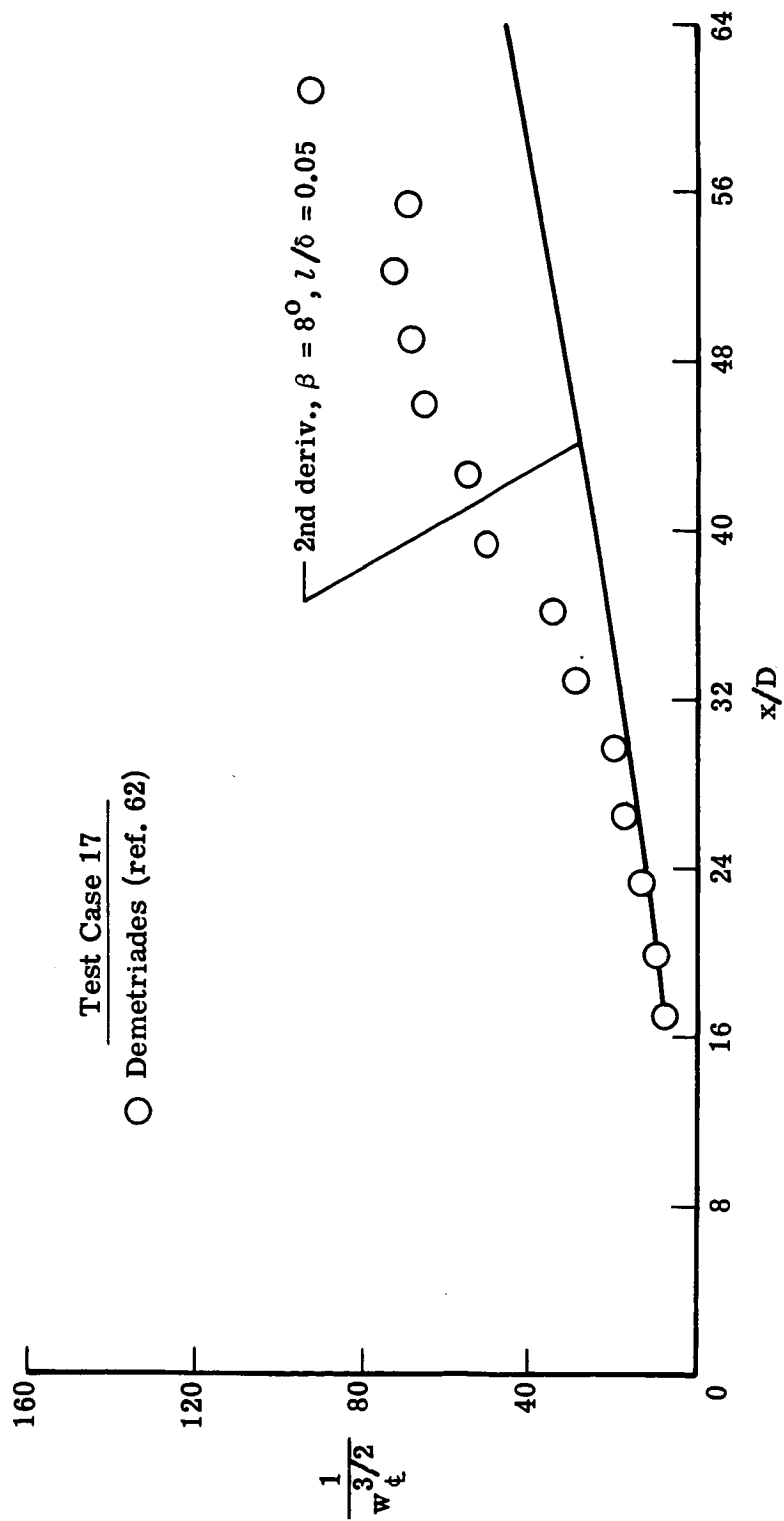


Figure 25.- Predicted and experimental center-line velocity for an axisymmetric supersonic wake. Test case 17.

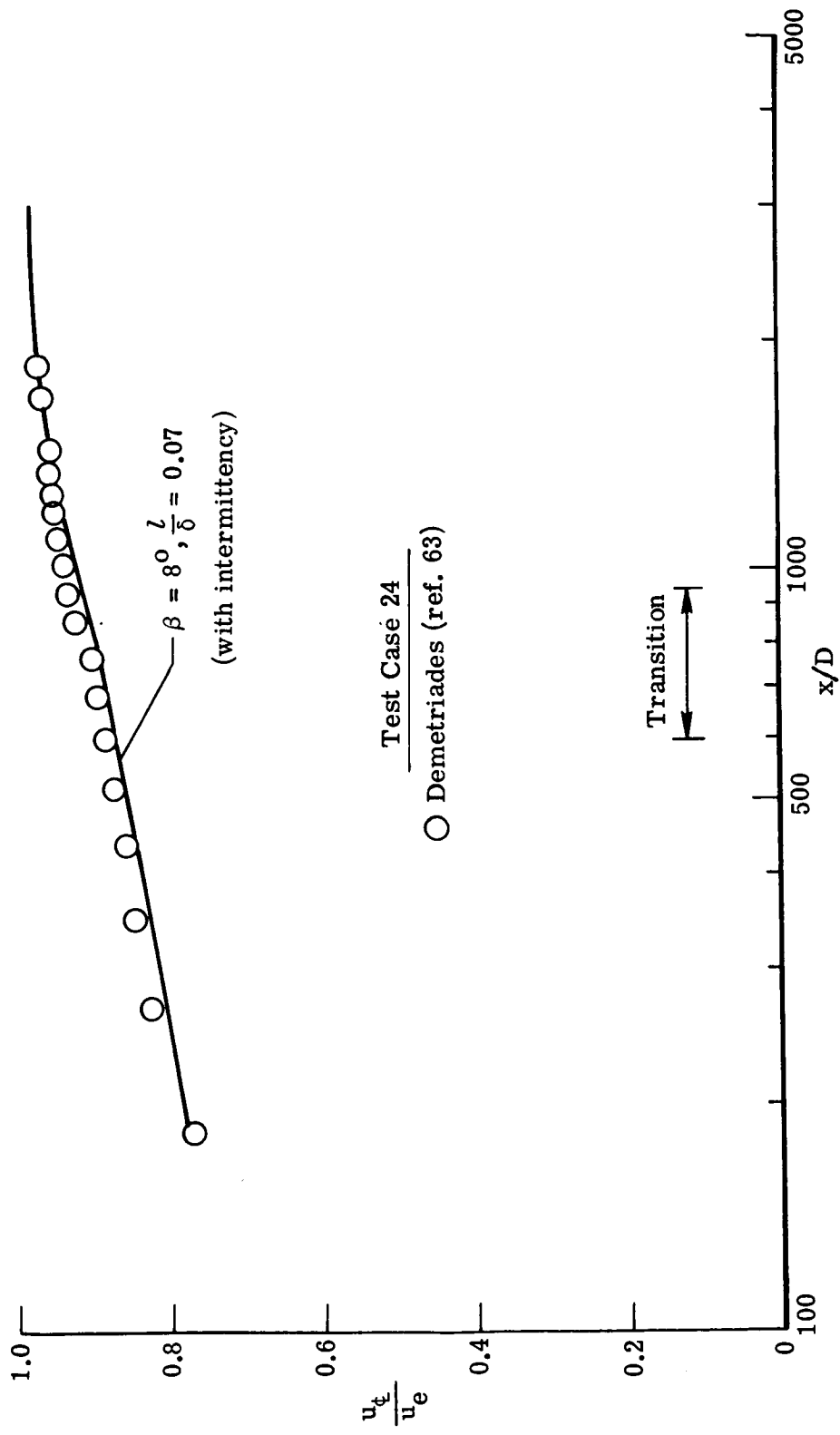


Figure 26.- Predicted and experimental center-line velocity for a two-dimensional supersonic wake. Test case 24.

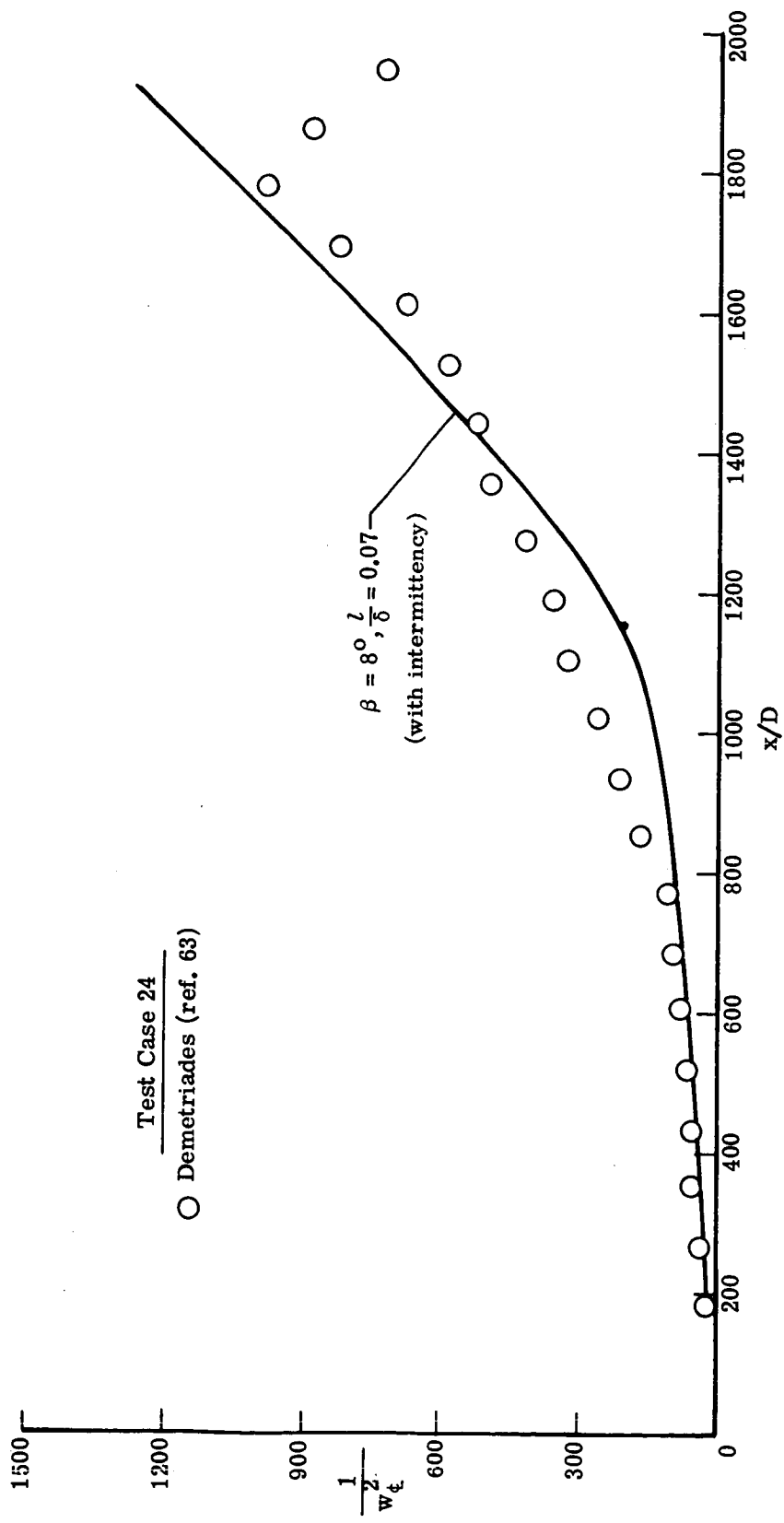


Figure 26.- Concluded.

DISCUSSION

H. McDonald: Can we regard this paper as a yardstick by which to judge the other predictions; in other words, if you cannot do any better than Prandtl's mixing length, then why bother? That is the first question I would like for you to try and answer. The second one is, are you advocating a development of Prandtl's mixing length and should this work be pursued, or do you think that this is the point at which to abandon the specific concept of mean field-direct relation with the turbulence and go on perhaps to the turbulence kinetic energy equation and multiequation models of turbulence?

D. H. Rudy: Since a length scale equation has been added to the basic mixing length model, the calculations cannot be regarded as baseline calculations in the classical sense. The Imperial College paper has that type of mixing length calculation. Our use of the mixing length is merely an attempt to better represent the physics of turbulent mixing in nonequilibrium flows. The Conference Evaluation Committee is of course best qualified to determine what this approach means in terms of other prediction methods. Personally, I think that approaches like the various "two-equation" models which incorporate a length scale equation appear promising.

D. M. Bushnell: We use this thing just as a tool to analyze the flows. We've used other tools before and the mixing length is a convenient handle to put on the flow to find out if it is doing anything surprising. I think it is obvious that you want to continue development and each method in the hierarchy has its own application, and I think I'll leave it at that.

V. W. Goldschmidt: I guess I have a similar question: What is the basis for determining whether the model works or not? Is it strictly a comparison with mean velocity or are we going to try to look at turbulence stresses as well? I think if we take that daring step your conclusions would have to be rephrased a little bit differently. Am I correct?

D. H. Rudy: Yes, we have examined only mean flow quantities and not the details of the turbulence which are of course more sensitive to modeling. Perhaps the Evaluation Committee will comment on this but I do agree with your observation.

H. McDonald: I'm sorry our time doesn't permit any more questions. I'd like to proceed if I may.

Written Comments

S. J. Kline: For many decades most workers, including the discussor, have had the idea that the mixing length and eddy viscosity were fundamentally different assumptions. However, recent developments suggest this is not so; there are two points. First, both are closures which depend only on the local mean strain and scaling on the layer width. Second, it follows from this that whenever one is used, there exists an equivalent formulation

which is wholly consistent and equivalent within the accuracy of this level of approximation. In the case of Rudy and Bushnell's formulation, for example, one can write

$$\tau = \frac{\rho l^2}{\delta^2} \delta^2 \left| \frac{\partial \bar{u}}{\partial y} \right| \frac{\partial \bar{u}}{\partial y} \quad (1)$$

If we also write

$$\tau = \rho \epsilon \frac{\partial \bar{u}}{\partial y} \quad (2)$$

and equate τ in equation (1) and equation (2), we have

$$\epsilon = l^2 \frac{\partial u}{\partial y} \approx l^2 \frac{\Delta U}{\delta}$$

and, since l is scaled on δ ($l/\delta = \text{Constant}$), this is equivalent to $\epsilon = k\delta \Delta U$. Thus, the differences observed in the two cases should arise from the forms and values taken for the constants, and not from a fundamental difference between mixing length and eddy viscosity formulations.

P. J. Ortwerth: The measured static-pressure defects which concern the authors have been analyzed by myself prior to the formulation of my model. An order of magnitude analysis shows that to first order the proper integration of the radial momentum equation becomes

$$\bar{p} + \overline{(\rho v)' v'} = p_e \quad (1)$$

and the normal velocity component remains a second-order term – that is,

$$\rho \bar{v}^2 \ll \overline{(\rho v)' v'} \quad (2)$$

Further, equation (1) has been subsequently verified by Roger Craig in our laboratory by comparing $\overline{\rho v'^2}$ measured with a hot wire anemometer, Thermo Systems model 1100, and measured static pressure on jets.